Impedance spectroscopy of brushite composites and a scaling approach to the dispersion behavior of inhomogeneous ionic conductors

L. Tortet, J. R. Gavarri, J. Musso, and G. Nihoul

Laboratory of Multiphase Materials and Interfaces, University of Toulon Var, Boîte Postal 132 La Garde Cedex, France

J. P. Clerc

Institut Universitaire des Systèmes Thermiques Industriels, University of Provence, Technopole de Château Gombert, Enrico Fermi 5, 13453 Marseille Cedex 13, France

A. N. Lagarkov and A. K. Sarychev

Scientific Center for Applied Problems in Electrodynamics, Russian Academy of Science, Izhorskay 13/19, 127412 Moscow, Russia

(Received 4 September 1997; revised manuscript received 17 February 1998)

The conductivity of composites prepared from ceramics is studied. The conductivity has an ionic character and the complex impedance behaves similar to many other inhomogeneous ionic systems. The dependence on the frequency is nonanalytical in form and can be described with some exponents that appear to depend on the concentration. We develop a Monte Carlo algorithm and perform a comprehensive computer simulation of the system. A network analysis reproduces the behavior of the complex impedance so that we can connect experimentally measured quantities to the internal structure of the system. Our theory predicts the values of the exponents and gives their dependence on the structure of a particular system. The most important parameter is the width of the distribution of the local conductivities. When the width increases, the exponents describing the frequency behavior reach universal values that are independent of the particular features of the system. The developed theory can be applied to understand impedance spectroscopy data for various inhomogeneous ionic conductors and some electronic conductors as well. [S0163-1829(98)00833-9]

I. INTRODUCTION

Impedance spectroscopy is a rather simple and very informative tool for studying various properties of inhomogeneous systems.[1] The impedance spectra of ionic conductors are especially interesting and important since the electric current flow in such conductors is accompanied by a mass transfer. This results in various physical and electrochemical processes: aging, diffusion limited impedance behavior (Warburg impedance), etc. (see Refs. 2–6, and references there in). On the other hand, numerous processes taking place in inhomogeneous ionic conductors make the interpretation of the impedance spectroscopy data a difficult problem. At this moment, there is neither an analytical theory nor comprehensive computer simulations that allow us to connect the measured spectra to microscopical properties of inhomogeneous ionic conductors. The effective properties of inhomogeneous ionic conductors are not only interesting physical problems but also the subject of great practical importance. Let us just mention a few examples. Many biological objects are essentially inhomogeneous ionic conductors. Solid and liquid inhomogeneous ionic conductors are the bases for various batteries. The conductivity and dielectric response of the brine-saturated rocks are also inhomogeneous ionic conductor problems.

In this paper, we consider a simple physical system that shares many features of inhomogeneous ionic conductors. We investigate the complex impedance $Z(\omega) = Z_1(\omega) + iZ_2(\omega)$ of the pellets prepared by compacting a powder of calcium dihydrated hydrogen-phosphates granules having chemical formula $CaHPO_4 \cdot 2H_2O$. This calcium dihydrated hydrogen phosphate has a monoclinic crystal structure with four molecules for an elementary cell and is known as brushite.[7] When dried, brushite is an insulator. However, when the pellets have been kept in a humid or ambient atmosphere, they have a well-defined conductivity. The conductivity of the "wet" composites may be attributed to a thin water layer adsorbed on brushite grains where some water molecules dissociate as, say, $H^+ + OH^-$, allowing charge transfer through the system.[8–10]

Experimentally we find that the frequency dependence of the complex impedance $Z(\omega)$ for the wet brushite samples has a form that has been associated for a long time with ionic conductivity for various inhomogeneous systems (see, e.g., Refs. 2–5, and references therein). It is often convenient to present impedance data in the form of the Nyquist plot, i.e., the parametric plot of $Z(\omega)$ in the complex plane $\{Z_1, Z_2\}$. Then the curve $\{Z_1(\omega), Z_2(\omega)\}$ looks similar to a depressed semicircle. Though this depression has been observed for a long time, this dispersive behavior is still poorly understood and there is no quantitative theory to connect the depressed semicircle dispersion to the microscopical structure of a system. In the absence of a proper theory, the complex impedance measurements can be used for engineering problems, but it is difficult to make definite conclusions about the internal structure of the inhomogeneous system. Usually the dispersion behavior of the complex impedance in ionic systems is well approximated by the following empirical equation:[1–5]

$$Z(\omega) \propto \frac{1}{1+(-i\omega\tau_1)^{\alpha_1}}, \tag{1}$$

where α_1 is some noninteger exponent sometimes called the Debye parameter[1,2] and τ_1 stands for an effective relaxation time. In general, these parameters depend on the observed system. It is quite reasonable to suppose that the effective relaxation time τ_1 is different for different systems; for some systems, it may also depend strongly on temperature (see, e.g., Ref. 2). What may seem more surprising is that the ''critical exponent'' α_1 also varies, from one to one half depending on the material. The term $(i\omega\tau_1)^{\alpha_1}$ even has a special name in electrochemical literature: The Cole element or a constant phase element (CPE).[2–5] The CPE was introduced in electrochemistry science to take into account the continuous distribution of electric equivalent circuits. Recently, Wang and Bates[11,12] have interpreted the $(i\omega)^{\alpha_1}$ behaviors as resulting from the distribution of activation energies E_{act} associated with a large variety of ionic jumps between two sites. A similar approach was proposed to simulate the electrode and interface electrical responses.[13]

To easily understand the origin of the $(i\omega)^{\alpha_1}$ behaviors experimentally observed in electrochemistry, it is necessary to recall that the effective local ionic paths (local electrical nets) can be built from (R,C) electrical local circuits having various values of R and C and linked together in parallel and in series. If the R, C values are statistically distributed with very different extreme values, then the macroscopic evolution is obviously characterized by a function having a variation ranging from pure conductive ω-independent behavior to pure capacitive ω-dependent behavior. This might be expressed by writing the macroscopic result as depending on ω^{α_1} with α_1 between 0 and 1.

Nonanalytical behavior of the form ω^{α} is typically for the response functions of an inhomogeneous system near the critical point where the size of inhomogeneity—the correlation length—goes to infinity. In our case, all characteristic times in the system are involved in the dispersion behavior.[14] As a first example, conductivity σ of classical percolating composites has the dispersion $\sigma(\omega)\propto\omega^{\alpha}$ for concentrations of the conducting component p close to the percolation threshold p_c. In this case the critical exponent α is equal to $\alpha=t/(s+t)$, where t is the critical exponent for the effective static conductivity $\sigma_e(p)$ just above the percolation threshold $\sigma_e(p)\propto(p-p_c)^t$, and s is another critical exponent governing the divergence of the effective dielectric constant $\varepsilon_e(p)$ near the percolation threshold $\varepsilon_e(p)\propto|p-p_c|^{-s}$ (see, e.g., Ref. 15). Critical exponents s and t are well defined and equal to 0.8 and 2.0, respectively, for three-dimensional (3D) percolating systems. Therefore, the critical exponent $\alpha \approx 0.7$ is also well defined for the classical 3D percolating composites. It follows from this that the 3D classical percolation theory cannot explain the variety of the indexes α in inhomogeneous ionic conductors.

This could be linked to quantum effects in real percolating composites with electronic conductivity: the static conductivity does not vanish immediately for concentrations p smaller than the percolation threshold $p<p_c$. In the absence of a conducting channel spanning through the system, the quantum tunneling of the electrons between finite conducting clusters leads to a finite bulk conductivity. Under such con-

ditions, the frequency behavior of the effective conductivity is different than the one obtained by classical percolation. Namely, the critical exponent α increases up to $\alpha \approx 0.90-0.98$ (see Ref. 16, and references therein). Such a prominent difference in dispersive behaviors for the classic and quantum systems is a consequence of the different distributions of local currents. For classical percolation, the spatial distribution of local currents is determined by the self-similar structure of the infinite cluster for all spatial scales less than the percolation correlation length ξ_p. On the other hand, the structure of local currents in the quantum tunneling percolating systems is determined by the spatial period ξ_t of the effective Abraham-Miller network.[16] For concentrations $p<p_c$, the period ξ_t—the tunneling correlation length—is much larger than the percolation correlation length $\xi_t\gg\xi_p \gg a_0$, where a_0 is the average grain size.[16] Therefore, we here have another example of the dispersive behavior of an inhomogeneous system where the critical exponent α has a well-defined unique value.

In each case, the critical dispersive behavior of the form $\sigma(\omega)\propto\omega^{\alpha}$ is achieved when the corresponding correlation length ξ is much larger than a microscopical scale.[14,15] Therefore, the critical dispersion of the complex impedance does not depend on particular microscopical features of the system. Let us recall that all critical systems can be divided into different classes of universality so that the critical exponents (α, for example) have unique values for each class. It follows from the above discussion that to explain the variety of the critical exponents α observed in ionic conductors, we have to assume that each of them should belong to a different class of universality.

Le Mehaute and co-workers in Ref. 5 have assumed that the total voltage drop across an inhomogeneous ionic conductor is determined by a voltage drop across some critical surface. In other words, the total resistance of the system is concentrated in the critical surface where the currents eventually cross on the way from one electrode to another. If this critical surface has a fractal structure, it is possible to show, using noninteger differential method,[5,17] that the complex impedance has the nonanalytical form given by Eq. (1). Then the critical exponent α depends on the fractal dimension of the hypothetical critical surface (''Le Mehaute surface''). Le Mehaute surfaces are supposed to have different fractal dimensions for different inhomogeneous ionic conductors: the different solid state ionic conductors considered in Ref. 5 belong to different classes of universality (see also Ref. 4, and references therein). Moreover, it was shown in Ref. 5 that the critical exponent α varies with temperature and time of storage (aging process) so that the systems should change their class of universality. The problem with such an interpretation of the nonanalytical dispersion behavior of ionic conducting systems is to connect the properties of the Le Mehaute surface, e.g., its fractal dimension, with the internal structure of the system. This problem has not yet been solved.

To complete this brief survey on dispersion behavior of the ac conductivity of the form $\sigma_1(\omega)\propto\omega^{\alpha}$, where the exponent α may depend on the parameters of the system, let us recall the behavior of amorphous semiconductors in the frequency range, say, 10 s$^{-1}<\omega<10^8$ s^{-1} (see, e.g., Ref. 18, and references therein). A fractional power law in the fre-

quency dependence of the dielectric response is also seen in various dielectric materials (see, e.g., Refs. 1 and 19). Numerous theoretical approaches to this problem have been developed.[1,18,19] Most of them are based on the one particle approximation when each electron is considered as independently interacting with an external electric field. Therefore, these approaches cannot be directly applied to ionic systems where the nonanalytical dispersion behavior of the complex impedance starts from very low frequencies and is essentially a collective process. Application of the one particle approach to the amorphous and heavily doped semiconductors is also somewhat controversial since the internal field does not necessarily coincide with the external one and may fluctuate strongly over the system. This problem may be especially important for systems with a giant effective dielectric constant (see, e.g., Ref. 20).

To understand the origin of this nonanalytical behavior of the complex impedance $Z(\omega)$, we have prepared brushite composites by adding polymer (polyphenylsulfur) particles to brushite grains. In this way, we introduce a well-controlled parameter, namely, the volume concentration q of polymer particles. When the polymer concentration q increases, the volume concentration of the brushite grains and pores $p = 1 - q$ decreases. Correspondingly, the effective static conductivity $\sigma_e(p)$ also decreases and vanishes at a concentration p equal to the percolation threshold p_c, which has been measured to be $p_c \cong 0.23$. As was stated above, the conductivity of the brushite-polymer system is due to the thin water layer adsorbed on brushite grains; it is then quite natural that the percolation threshold takes the value $p_c = 0.23$, which is typical for 3D percolating composites.

The anomalous dispersion of the complex impedance $Z(\omega)$, shown in Eq. (1), takes place for all studied concentrations, from $p = 1$ down to the percolation threshold $p_c = 0.23$, but the parameters of the dispersion curve change dramatically. First, the onset of the anomalous dispersion shifts toward smaller frequency by many orders of magnitude when the concentration p decreases. That is, the effective relaxation time τ_1 increases toward the percolation threshold. Then the critical exponent α_1 also changes with concentration. This behavior of the complex impedance $Z(p,\omega)$ is quite unusual. Since the brushite grains are responsible for the effective conductivity $\sigma_e(p,\omega)$ of the composites, we could expect, in agreement with percolation theory,[15] that $Z(p,\omega)$ is just proportional to some function of the concentration $Z(p,\omega) \propto z_b(\omega)f(p)$. The impedance $z_b(\omega)$ has the meaning of the impedance of a brushite grain (or contact between the grains), while the function $f(p)$ is such that $f(1) = 1$ for $p = 1$ and there is an asymptotic behavior $f(p) \propto (p - p_c)^{-t}$ for p close to the percolation threshold p_c. Therefore, the frequency dependence of the impedance $Z(p,\omega)$ should be the same for all concentrations $p_c < p \leqslant 1$. It could be argued that, for sufficient high frequencies, the displacement currents flowing in the dielectric grains and pores should be taken into account. Nevertheless, this cannot change, under any circumstance, the relaxation time τ_1 in Eq. (1) by several orders of magnitude.

The paper is organized as follows. First we consider the conductivity of the brushite composites on the microscopical level and find the most plausible pattern of the local conductivity distribution. The obtained local conductivities are then

used in a computer simulation of the system. A special and extremely effective numerical method which we call exact numerical renormalization has been developed to calculate the complex impedance of the brushite composites. The results of our computer simulations allow us to develop a scaling theory of the effective complex impedance $Z(\omega)$. The theory describes the dispersive behavior and explains the dramatic changes of the relaxation time τ with concentration p. It appears that there are two "critical" exponents in the system. One is α_1 which can be found in Eq. (1) and the other α, which governs the behavior of the impedance or of the effective conductivity $\sigma_e(\omega) \propto \omega^\alpha$ in the high frequency limit $\omega \gg 1/\tau_1$. Correspondingly, there are two time scales, τ_1 and τ. The impedance dispersion follows Eq. (1) for the frequencies $\omega \propto 1/\tau_1$, and switches to asymptotic behavior $\sigma_e(\omega) \propto \omega^\alpha$ for $1/\tau_1, \ll \omega \propto 1/\tau$. Our theory gives strong evidence that exponents α_1 and α take their universal values $\alpha_1 \approx 0.86$ and $\alpha = 1$ in the limit of strong disorder.

Under different conditions, the exponents α_1 and α are just some fitting parameters that can be used to approximate the effective impedance behavior as a function of the frequency ω. Yet, the dispersive behavior of the impedance $Z(\omega)$ is very well fitted by the nonanalytical frequency dependence $Z(\omega) \propto \omega^\alpha$ when changed by many orders of magnitude. We propose a scaling equation for the complex impedance $Z(\omega)$ that reproduces its dispersion behavior in the entire frequency range.

We then briefly describe the experimental method and compare the experimental data with theory. It appears that the analytical equation obtained from the computer data well reproduces the dispersive behavior of the complex impedance $Z(p,\omega)$ obtained in the experiment. We obtain the dependence of the exponents α_1, α and the effective relaxation rates τ_1, τ on the concentration of the conducting grains p and other parameters of the system such as temperature, for example. Finally, we show in the discussion that the main features of the dispersive behavior of many others inhomogeneous ionic conductors can be explained qualitatively from the approach developed in this paper as soon as a local conductivity can be defined.

II. MICROSCOPICAL CONSIDERATIONS ON THE LOCAL CONDUCTIVITY

Let us start by studying the origin of charge transfer in brushite composites. Dried brushite composites have a conductivity close to zero. If kept at room conditions or, better, in a humid atmosphere, they acquire a well-defined conductivity. For example, the pure brushite composite ($p = 1$) has a low frequency conductivity of 1.1×10^4 sec^{-1} (here and in the rest of the paper we use cgs units). It has been shown that what is observed is the conductivity of the thin water layer adsorbed on the brushite grains.[14] The adsorbed water has been measured as 0.01–0.02 % (by weight) of the bulk composite. Taking into account the average size of the brushite grains ($a_0 \cong 1.8 \times 10^{-3}$ cm) and the density of the brushite ($\rho_b = 2.31$ g/cm^3) we obtain the average thickness of the water layer, $d_0 \sim 10^{-7}$ cm. Since the average distance between molecules of water l_0 is equal to $l_0 \cong 3 \times 10^{-8}$ cm (Ref. 21) the adsorbed water layers are only a few molecules thick. Depending on the humidity rate, these layers might be more

or less discontinuous. Dykhne proposes[22] that for a low humidity rate the water does not cover the brushite grain in a continuous film but forms ''lakes'' on its surface. The lakes may have ramified structure due to the inhomogeneities of the surface. Obviously, only lakes common to 2 grains participate in the global conductivity. When the humidity increases, the water lakes grow as well as the contact area. Finally, the adsorbed water on one grain forms an infinite percolating cluster and the brushite grain reaches the effective surface conductivity σ_g as it takes place in our experiment.

Let us now study this σ_g conductivity. We assume that the conductivity of the water layer is mostly determined by proton conductivity and allowing the relaxation distance for a proton to be about l_0, we obtain that the proton concentration in the layer is about $n_p \cong 8 \times 10^{14}$ cm^{-3}. In other words, there are about 10^9 protons per square centimeter of the brushite grain. Such a significant concentration of protons can be linked to the fact that the effective energy $E^s_{H_2O}$ for dissociation of the water molecule $H_2O \rightarrow H^+ + OH^-$ is much smaller on the brushite surface than E_{H_2O} in bulk water. Correspondingly, the proton concentration $n_p \propto \exp(-E^s_{H_2O}/2T)$ is much enhanced with respect to the bulk water. We can write the following chemical equation for the equilibrium state: $H_2O(\text{adsorbed}) \leftrightarrow H^+(\text{surface}) + OH^-(\text{adsorbed})$, from which it follows that the effective dissociation energy is equal to $E^s_{H_2O} \cong E_{H_2O} + D_{H_2O} - D_{HO} + D_H$, where D_{H_2O}, D_{HO}, and D_H are the surface energies for the water molecules, hydroxyl ions, and protons, respectively. The brushite grains have acid properties and strongly attract hydroxyl ions. As a first approximation, the energy E_{H_2O} needed to separate OH^- from H^+ in bulk and the energy needed to separate OH^- from the surface of the grain might be considered as similar: D_{HO} should be close to E_{H_2O}. A specific mechanism of the surface reactions has been proposed in Ref. 23 where the energy D_{HO} is given, which is almost equal to the dissociation energy E_{H_2O} (in the bulk), while the energy D_H is about the energy of a hydrogen bond, i.e., $D_H = 0.1 - 0.3$ eV. The adsorption energy D_{H_2O}, as follows from our experimental data, is small and is of the order of room temperature. From the above discussion, it follows that the surface dissociation energy $E^s_{H_2O}$ is much smaller than the bulk value E_{H_2O} and consequently, the concentration n_p of the protons is strongly enhanced in the surface layer. As soon as a proton is dissociated from a water molecule, it can move rather freely over the surface of the brushite grain. The activation energy for surface motion E_p is in general less than the affinity energy D_H. Note that we do not take into account the direct Coulombic interactions between charged particles since the average energy of that interaction $e^2 \sqrt{n_p d_0} \sim 10^{-2}$ eV is less than other characteristic energies, including the thermal energy at room temperature.

All the above estimations are very crude since the surface of the brushite grains is inhomogeneous: the thickness of the water layer as well as the energy of dissociation $E^s_{H_2O}$, the affinity energy D_H, and the activation energy E_p fluctuate over the surface. Because the ratio is $E^s_{H_2O}(\mathbf{r})/kT \gg 1$, one can write the local proton concentration as $n_p(\mathbf{r}) \sim \exp$

$[-E^s_{H_2O}(\mathbf{r})/2kT]$. Hence, the local surface conductivity $\sigma_g(\mathbf{r}) \sim n_p(\mathbf{r}) \exp[-E_p(\mathbf{r})/kT]$ fluctuates strongly over the brushite surface. Note that the Debye radius r_D estimated from the average proton concentration n_p is small enough ($r_D \sim 4 \times 10^{-7}$ cm) to warrant the introduction of local conductivity $\sigma(\mathbf{r})$. We will not discuss the problem of the conductivity of a single brushite grain in detail. Instead, we prescribe it some effective conductance σ_g that is assumed to be more or less the same for all the grains in average.

The effective conductivity σ_e of the brushite composites is then determined mostly by the contacts between different brushite grains (3D percolation). The excitation energy E_c for a proton jumping from one brushite grain to another is about (or larger than) the affinity energy $E_c \gtrsim D_H$ so that $E_c/kT \gg 1$. The contacts between the brushite grains have different sizes and shapes and the affinity energy D_H is subject to strong fluctuations. It would appear reasonable that the jumping energy E_c fluctuates strongly from contact to contact. Therefore, the contact conductivities $\sigma_i \propto \exp(-E_c/kT)$ are distributed in an exponentially wide range of magnitudes. We adopt the simplest possible assumption that the jumping energy E_c is distributed uniformly in some interval ΔE_c around the average value E_{c0}. Then the contact conductances Σ_i can be rewritten in the following form:

$$\Sigma_i \cong \Sigma_0 \exp(-\lambda x_i), \qquad (2)$$

where the prefactor Σ_0 is equal to $\Sigma_0 \propto \exp[-(E_{c0} - \Delta E_c/2)/kT]$, the dimensionless parameter λ is E_c/kT and is large $\lambda \gg 1$ (as kT at room temperature is 2.5 meV), and random parameters x_i take values in the range $0 < x_i < 1$.

It is possible to show[20] that any interstitial defect in the inhomogeneous conductors gives rise to a corresponding capacitance switched in parallel to the interstitial conductance. This capacitance appears to be independent of the interstitial conductance. In our case, it is the capacitance of the contact between two brushite grains. If we take into account the contact capacitance, we obtain that for finite frequency ω the contact conductance Σ_i now becomes

$$\Sigma_i(\omega) \cong C \left[-\frac{i\omega}{4\pi} + \sigma_0 \exp(-\lambda x_i) \right], \qquad (3)$$

where the geometrical factor C has dimension of length (remember that in cgs units a capacitance has length dimension) and $\sigma_0 = \Sigma_0/C$. To simplify, we assume that the factor C is the same for all brushite-brushite contacts. Finally, one should take into account the bulk dielectric constant ε of the brushite composites. This quantity becomes important when the frequency ω exceeds the value of the characteristic contact conductivity σ_0 and the brushite grains become disconnected effectively.

The electric current in the ionic system is accompanied generally by a mass transfer. In our particular system, the cations (most probably protons) discharge at the cathode and form, e.g., hydrogen molecules that may escape from the system. To compensate for the deficit of the cations some diffusion flow of the cations should come to the cathode. Suppose that τ_d is the characteristic time for the diffusion process. When the frequency ω of the external electric field is larger than the characteristic diffusion frequency $\omega > 1/\tau_d$ the diffusion processes are unimportant since the cathode and anode switch places too fast for any transfer to take

place. For frequencies $\omega < 1/\tau_d$ the diffusion imposes additional restrictions on the number of discharged particles and, therefore, on the current flowing through the system. We will not consider the diffusive limited conductivity (Warburg impedance)[24] and restrict ourselves to the frequencies $\omega > 1/\tau_d$ in this paper.

III. COMPUTER SIMULATION: PHYSICAL MODEL OF BRUSHITE COMPOSITES AND EXACT NUMERICAL RENORMALIZATION METHOD

A. Physical considerations

In the previous section, we proposed that contact conductances between the brushite grains should be distributed according to Eq. (3). Such an exponential distribution of the local conductivities $\sigma(\mathbf{r})$ is common for many inhomogeneous ionic conductors, provided that the notion of local conductivity has a meaning. Indeed, the charge transfer in the ionic conductors is typically an activation process. The local activation energy $E_c(\mathbf{r})$ is usually much larger than the thermal energy T and fluctuates over the inhomogeneous ionic system. Therefore, the local conductivity fluctuations can be written as $\sigma(\mathbf{r}) \sim \exp[-E_c(\mathbf{r})/kT]$.

To calculate the effective conductivity of the brushite composites and obtain insight into the dispersion behavior of the system with the exponentially distributed local conductivities, we arrange elements with conductances given by Eq. (3) in a cubic lattice. Thus we obtain the following system for a computer simulation: each bond of the cubic lattice can be either broken or has conductivity

$$\sigma_i = -i \frac{\omega}{4\pi} + \sigma_0 \exp(-\lambda x_i), \qquad (4)$$

with parameter $\lambda \gg 1$ and x_i distributed uniformly between 0 and 1. Note that we skip the geometrical factor C in Eq. (4) in comparison with Eq. (3) since it is assumed to be the same for all conducting elements and consequently does not affect the dispersion behavior of the effective complex conductivity. The broken bonds in the cubic lattice represent the polymer grains and their conductivity is assumed to be zero. This simple computer model does not include the conductance of the brushite grain, the capacitive conductance of the polymer grains, etc. These quantities should fluctuate much less than the contact conductivities, hence, they cannot qualitatively change the dispersive behavior which we are interested in. In Sec. V, we will discuss some of these complexities in the scaling theory when we compare the experimental data with our computer results.

Thus, we have a percolating system where the real part of the conducting elements is distributed in an exponentially large range $\sigma_0 \exp(-\lambda) \leq \mathrm{Re}(\sigma_i) \leq \sigma_0$, $\lambda \gg 1$. Below, we will measure the frequency ω and effective conductivity σ_e in terms of σ_0. Then the dimensionless conductivity of the conducting bond takes the following form:

$$\sigma_i = -i\omega' + \exp(-\lambda x_i), \qquad (5)$$

where $\omega' = \omega/(4\pi\sigma_0)$ is the reduced frequency. We use a random number generator to put the conducting bonds with probability p and broken bonds with probability $1-p$ in the cubic lattice. Then, again, we use a random number genera-
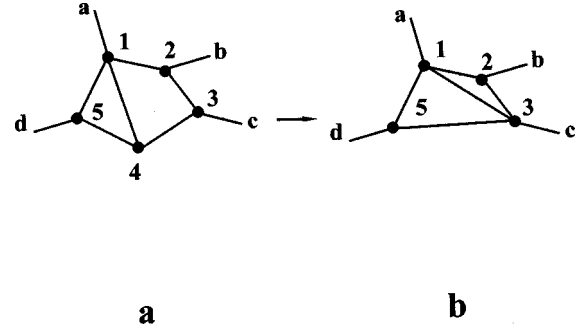

FIG. 1. Exact numerical renormalization (ENR) procedure for decimating site 4. Note that the number of neighbors of site 3 increases from 2 to 3.

tor to generate the random numbers x_i and obtain the conductivities of the conducting bonds according to Eq. (5).

We now have to introduce the external electric field $\mathbf{E} = \{E_x, E_y, E_z\}$ in the computer simulations. The Kirchhoff equations used to find the effective conductivity are obtained by discretizing the charge conservation law $\nabla \cdot \sigma(\nabla\varphi_1) = 0$, where φ_1 and σ are the local potential and conductivity on the mesh. The charge conservation law can also be written as $\nabla \cdot \sigma(\mathbf{E} - \nabla\varphi) = 0$, where $\mathbf{E}$ is an external electric field while φ is the fluctuating potential with volume average $\langle \nabla\varphi \rangle = 0$. When we discretize this equation on a cubic lattice the external field is represented by batteries in series with each conducting bond: their electromotive forces (EMF's) will be equal to E_x for x bonds, E_y for y bonds, and E_z for z bonds. The introduction of the external electric field by EMF's included in all conducting bonds allows us to set cycle boundary conditions in all directions. Thus, our finite size percolating systems have no boundaries at all: finite size effects are much reduced for cycle conditions in comparison with other approaches discussed in the literature.[15,24–26] Note that the equation $\langle \nabla\varphi \rangle = 0$ and its discretization on the lattice are fulfilled automatically for the chosen boundary conditions.

The simulation of a three-dimensional percolating system with exponentially distributed local conductivities is a difficult computer problem since we should consider a system large enough to achieve the statistical limit. To tackle the problem we have developed an algorithm which we call exact numerical renormalization (ENR). This algorithm can be considered as an outgrowth of Refs. 26 and 27.

B. Computer simulations

To gain insight into the ENR method, let us first consider a simple system of five conducting sites as shown in Fig. 1. We write the charge conservation law, the Kirchhoff equations, for each site i shown in Fig. 1 in the following form:

$$\sum_j \sigma_{ij}(\phi_j - \phi_i + E_{ij}) = 0, \qquad (6)$$

where ϕ_i is the potential of a site i, σ_{ij} is the conductivity of the bond between the sites i and j, and E_{ij} is the EMF included in the bond $\{i,j\}$ representing the external field. The summation in Eq. (6) goes over all j sites that are neighbors to the site i. From Eq. (6), we can express the potential of a
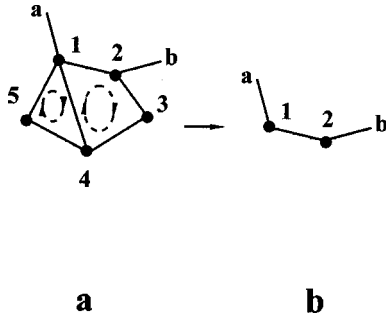
a   **b**

FIG. 2. Exact numerical renormalization procedure for decimating sites 3 and 4. The response to an external field or current is the same in (a) and (b), but the dissipation due to the loop currents (1-4-5) and (1-2-3-4) is lost.

particular site ϕ_k in terms of the potentials of the other sites. Thus, e.g., the potential ϕ_4 of site 4 in Fig. 1 is equal to

$$\phi_4 = \frac{\Sigma_j \sigma_{4j}(\phi_j - E_{4j})}{\Sigma_j \sigma_{4j}}, \tag{7}$$

where the summation is over all neighbors of site 4, that is, the index j takes values $\{1,2,3,5\}$. The potential ϕ_4 appears in the Kirchhoff equations for site 4 and for its neighbors. Substituting ϕ_4 given by Eq. (7) we exclude the potential ϕ_4 from the total set of Kirchhoff equations. Thus, we exclude site 4 from the system. The conductivities of the bonds between the neighbors i and j of the excluded site 4 change under this transformation taking new values

$$\sigma_{ij}^* = \sigma_{ij} + \frac{\sigma_{i4}\sigma_{4j}}{\Sigma_j \sigma_{4j}}, \tag{8}$$

where the summation is still over all neighbors of site 4. Note that even disconnected neighbors 1 and 3 of site 4 ($\sigma_{13} = 0$) are connected now: the sites that were connected indirectly via site 4 become connected directly after the elimination of this site. This decimation process is a generalization of the nodal method.[28]

The EMF's E_{ij} that were standing in the bonds of the original system also change after the elimination of site 4. EMF E_{ij}, standing in a bond between neighbors i and j of eliminated site 4, takes the new value

$$E_{ij}^* = E_{ij}\frac{\sigma_{ij}}{\sigma_{ij}^*} + \left(1 - \frac{\sigma_{ij}}{\sigma_{ij}^*}\right)(E_{4j} - E_{4i}), \tag{9}$$

where σ_{ij}^* is given by Eq. (8). The new values E_{ij}^* of EMF's depend on the initial EMF's E_{ij} but also on EMF's E_{4j} and E_{4i} which stood in the bonds $4i$ and $4j$.

Thus instead of the initial system of five sites shown in Fig. 1(a) we obtain the new renormalized four-site system shown in Fig. 1(b). Since the transformations given by Eqs. (8) and (9) are exact, the new system is equivalent to the initial one: the response of both systems to the currents and voltages applied to the external terminals $\{a,b,c,d\}$ is the same. However, the energy dissipation between original and renormalized systems is different. When we remove a site from the system, we lose the dissipation associated with the circular currents flowing through the eliminated site. We illustrate this in Fig. 2, where the site configuration is almost

the same as in Fig. 1, but sites 3 and 5 have no external terminal. After decimation of sites 3–5, we lose the dissipation due to mesh currents. Yet, the response to an external signal is the same for the diagrams in Figs. 2(a) and 2(b). By solving the Kirchhoff equations it may be shown that the difference in the energy dissipation Q in the original and renormalized systems is independent of the voltages applied to the external terminals. Thus, for the diagrams shown in Figs. 1(a) and 1(b), the difference in the dissipation Q_4, arising due to the decimation of site 4, is given by the following equation:

$$Q_4 = \sum_{i,j} \frac{(E_{4i} - E_{4j} + E_{ij})^2 \sigma_{4i}\sigma_{4j}\sigma_{ij}}{\sigma_{4i}\sigma_{4j} + \sigma_{ij}\Sigma_k \sigma_{4k}}, \tag{10}$$

where the summations over indexes i, j, and k are still over all neighbors of the eliminated site 4. The system of Eqs. (8)–(10) forms the closed system of our ENR procedure.

To calculate the conductivity of the percolation system discussed above we apply ENR transformations, site by site, to the system. Since we use full cyclic boundary conditions, we remove all the sites from the system. When eliminating site m, we calculate the dissipation Q_m connected to the circular currents flowing through this site using Eq. (10). When all the sites are eliminated by means of the ENR procedure, we obtain the full dissipation in system Q by adding all local dissipations:

$$Q = \sum_m^N Q_m, \tag{11}$$

where N is the total number of sites. Then the effective conductivity of the system σ_e comes from the following equation:

$$\sigma_e E_0^2 = Q, \tag{12}$$

where $E_0^2 = E_x^2 + E_y^2 + E_z^2$ is the square of the external field.

In practical calculations, we put the amplitude of the external field $\mathbf{E}_0$ equal to $\mathbf{E}_0 = \{1,1,1\}$ for dc as well as ac current. In the former case, local conductivities σ_{ij} together with effective conductivity σ_e ascribe complex values and parameter Q loses the meaning of energy dissipation. Since we consider a quasistatic case, Eqs. (8)–(10) still hold for ac current. Moreover, it is easy to verify that Eqs. (11) and (12) still give the complex effective conductivity σ_e.

Let us now consider how the ENR procedure works for a system at percolation threshold when the infinite conducting cluster is strongly ramified and has a blob-link structure.[15] When we eliminate site m from the system by ENR, the number of neighbors for the other sites in general increases since the sites connected indirectly via site m now have a direct connection to each other. For example, the decimation of site 4 increases the number of neighbors for site 3 in Fig. 1 from 2 to 3. In a regular lattice, the application of ENR will lead to an exponential increase of the bonds per site. Therefore the number of operations (and computer time) for one site decimation increases with the number of eliminated sites. The situation changes near the percolation threshold due to the characteristic blob-link structure of the infinite cluster. Consider a blob of size L consisting of sites that are connected by conducting bonds [see Fig. 3(a), where four
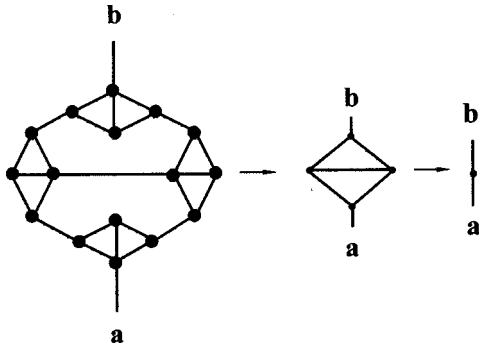
FIG. 3. Exact numerical renormalization procedure applied to the blob-link structure of the infinite percolating cluster. In the first step of ENR we decimate all blobs with sizes from 1 to L (a) and (b). In the next step, the blobs with size from L to $2L$ are eliminated (b) and (c).

blobs are represented]. Suppose that the blob is connected to the rest of the percolating system by two bonds only. If we eliminate all sites of the blob but one by ENR, this last site has two neighbors. Note that the result of exact renormalization does not depend on the internal structure of the eliminated blob. We can apply exact renormalization to all blobs of size L, reducing each of them to one site. Due to the self-similar structure of the backbone of the infinite cluster,[15,26,29,30] the resulting structure repeats the structure of the initial backbone, but the distance between new sites increases from 1 to L. The ENR applied to a self-similar backbone of an infinite conducting cluster is illustrated by Fig. 3(b).[26] When we reduce all blobs of size L using the ENR procedure, the structure of the blobs of size $2L$ is substantially simplified. At the next steps of ENR, we can eliminate blobs of size $2L$ and so on, until the size L_0 of the whole system is obtained [see Fig. 3(c)]. In practical calculations we do not bother to simplify the system before we start the ENR procedure. Thus we do not eliminate the finite clusters in the system or extract a backbone from an infinite cluster since we have found that ENR decimates all the sites very quickly.

It follows that the ENR procedure requires $N \propto L_0^d$ operations to decimate all the sites in a percolating system of size L_0 and dimensionality d and, consequently, to calculate its effective conductivity. We can compare this estimate with the number of operations in other exact methods: the transfer matrix method[15] takes about $N \propto L_0^7$ operations and the Frank-Lobb algorithm[25] takes $N \propto L_0^4$ operations, however, this algorithm works for 2D systems only. For example, the ENR procedure takes about five minutes on a computer such as a Pentium 200 to calculate the effective conductivity of a percolating system with size $128 \times 128 \times 128$ and concentration p close to the percolation threshold.

To test the ENR we have calculated the conductivity of a percolating system with identical conducting bonds at the percolation threshold for different system sizes $L_0 = 16, 32, 64, 128$. The conductivity was averaged over 6400, 1600, 400, and 100 trials, respectively. From these calculations we estimate the critical exponent t for the conductivity using finite size scaling.[15] Thus, we obtain $t = 2.05 \pm 0.01$ which is close to the known value $t = 2.0$. Note, however,

that the system size and number of realizations in our calculations are larger than in all previous works that we know of.

We point out that the self-similar blob-link structure of the infinite percolating cluster, sketched in Fig. 3, is an approximation designed to represent geometrically the fundamental property of scale invariance of a physical system near a critical point.[14] The scale invariance—''scaling'' of the critical systems is a well-adopted hypothesis that is the basis of the modern theory of critical phenomena. However, it is very difficult to observe this scaling directly in experiments or computer simulations. Now we can reverse the above arguments and conclude that the exiting efficiency of the ENR procedure can be considered as a confirmation of the self-similar structure of the infinite cluster as well as finite clusters in a percolating system. Therefore, the success of ENR shows that a percolating system is scale invariant at the percolation threshold. Yet, the system does not remain the same in the process of ENR. The average number of conducting bond per site N_c increases gradually starting from $N_c \cong 2$ and achieving $N_c \cong 6$ at the last stages of the numerical renormalization of the system with size $L_0 = 128$. This just means that we cannot find an exact *analytical* renormalization procedure for our percolating systems (and other critical phenomena). Alternatively, if we want to keep N_c constant during the decimation, we have to work with a dimension d larger than (or equal to) the critical dimension $d_c = 6$.

The ENR procedure can still be used far away from the percolation threshold. For concentrations of the conducting component $p \lesssim 1$, the ENR procedure cannot remove all the sites. Nevertheless, the elimination of only a part of the sites increases the number of neighbors in the rest of the sites. The renormalization of bond conductivities in the system is another important result of ENR. In other words, ENR increases the connectivity of the system and mixes conductivities of the conducting bonds. Therefore it smoothes the original exponential distribution of the local conductivities given by Eq. (4). After applying the ENR procedure, we can successfully use the well-known relaxation method (see, e.g., Ref. 24) to find the effective conductivity of the system with $p \lesssim 1$. Otherwise, the convergence of the relaxation method cannot be achieved in the original system if the parameter λ in Eq. (4) is greater than $\lambda \gtrsim 5$.

IV. RESULTS OF THE COMPUTER SIMULATION AND SCALING THEORY FOR THE DISPERSIVE BEHAVIOR OF INHOMOGENEOUS IONIC CONDUCTORS

A. Power-law dispersion of the complex impedance in the entire concentration range

In this section, we present the results of the computer simulation of a 3D percolating system, namely, the cubic lattice with a concentration of conducting bonds equal to p, the other bonds being broken. Randomly distributed conducting bonds, representing the contacts between brushite grains, have conductivities distributed over an exponentially large range according to Eq. (5). We neglect polarization of the polymer grains in comparison with the contact conductances and put the conductivity of the ''dielectric'' equal to zero even at finite frequency. The parameter λ in Eq. (5) has been chosen to be equal to $\lambda = 10$, which corresponds
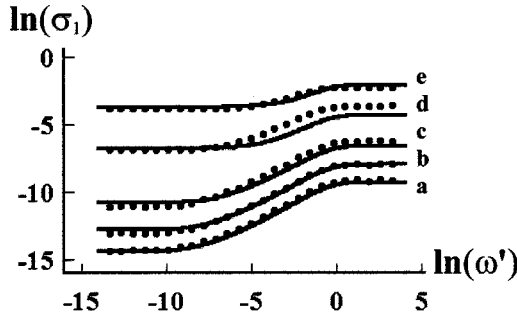
FIG. 4. Real part of the effective conductivity σ_1 obtained from computer simulations as a function of the reduced frequency ω' for different concentrations of the conducting bonds p: (a) $p=0.26$, (b) $p=0.27$, (c) $p=0.3$, (d) $p=0.5$, (e) $p=1.0$.

FIG. 6. Exponent α for the dispersion of the effective conductivity $\sigma_e \propto \omega^\alpha$. ●: computer simulations, ◆: result of estimation according to Eq. (25).

roughly to the experimental conductivity distribution in the brushite composites as will be shown in the next section. In fact, the main conclusions of this section do not depend on the particular value of the parameter λ as soon as $\exp(\lambda) \gg 1$. We use the ENR method described in the previous section to calculate the effective complex conductivity $\sigma_e = \sigma_1 - i\sigma_2$ for this model. The results for the effective conductivity $\sigma_1(\omega')$ and the reduced dielectric constant $\varepsilon(\omega') = \sigma_2(\omega')/\omega'$ are shown in Figs. 4 and 5, respectively, as functions of reduced frequencies ω' [see the discussion at Eq. (5)], for different concentrations p. Remember that the percolation threshold is equal to $p_c = 0.2493...$ (Ref. 15) for the bond percolation problem defined on the cubic lattice.

The real part of the effective conductivity $\sigma_1(\omega')$ (see Fig. 4) increases by many orders of magnitude with increasing frequency ω'. In the frequency region where $\sigma_1(\omega')$ increases significantly its dependence on the frequency can be well approximated by the power-law equation $\sigma_1(\omega') \propto \omega'^\alpha$. We determine that the ''critical exponent'' α as the maximum value of the slope, i.e., $\alpha(p) = \max\{\partial \ln[\sigma(p,\omega')]/\partial \ln(\omega')\}_{\omega'}$. Thus the defined exponent $\alpha(p)$ increases from $\alpha \cong 0.4$ for $p=1$ to $\alpha \cong 0.75$ for $p \to p_c$ as shown in Fig. 6. Such an increase of the critical exponent α is in qualitative agreement with the experimental data, as we will see.

We can see from Fig. 4 that the onset of the power-law behavior shifts about five orders of magnitude toward small frequencies when the concentration p decreases from $p=1$ to the percolation threshold p_c. This significant shift of the
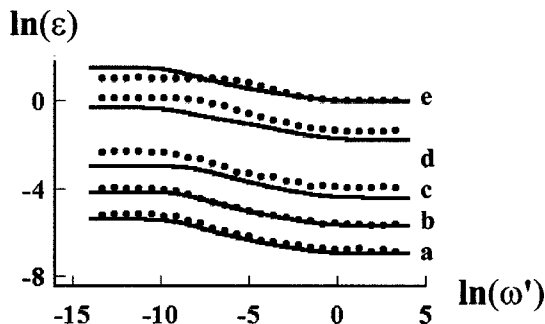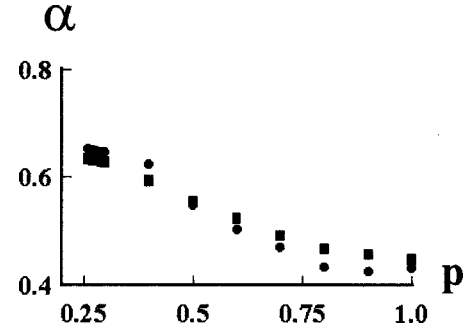
onset of the dispersion $\sigma_1(\omega') \propto \omega'^\alpha$ is also in qualitative agreement with our experimental data discussed in the next section. We also determine that the effective relaxation time τ_1 is the inverse proportional of the frequency ω'_0, where the imaginary part of the complex resistivity $\rho_2(\omega') = \sigma_2(\omega')/[\sigma_1^2(\omega') + \sigma_2^2(\omega')]$ is a maximum: this approximately corresponds to the onset of the dispersion of $\sigma_1(\omega')$. Thus, the defined relaxation time τ_1 increases exponentially as the concentration p decreases, as shown in Fig. 7.

Finally, in Fig. 8 we present the reduced effective complex resistivity $\rho'(p,\omega') = \rho(p,\omega')/\rho(p,0) = \rho'_1(p,\omega') + i\rho'_2(p,\omega')$ in the form of the Nyquist plot. The impedance diagram shows a well-defined depressed semicircle with the so-called damping parameter $\beta = \max_{\omega'}[\rho'_2(p,\omega')/\rho(p,0)] \cong 0.4$. Note that the points for all concentrations collapse to a single curve though the frequency behavior of the effective conductivity $\sigma_e(p,\omega')$ are quite different for different concentrations. This discrepancy may be understood if we recall that both α and τ depend on the concentration p (see Fig. 4). Let us also note that Nyquist plots lose information when compared to frequency dependence. The Nyquist plot in Fig. 8 can be approximated by the well-known empirical equation (1) (see Refs. 1–5) which can be written in the following form:

$$\rho'(\omega') = \frac{\rho(0)}{1 + (-i\omega'\tau_1)^{\alpha_1}}. \tag{13}$$

Then we find that the exponent $\alpha_1 \cong (4/\pi)\arctan(2\beta) \cong 0.86$ whatever p. Therefore, there are two relaxation time scales, τ_1 in Eq. (13) and τ, which corresponds to the maximum

FIG. 5. Effective dielectric constant ε obtained from computer simulations as a function of the reduced frequency ω' for different concentrations of the conducting bonds p: (a) $p=0.26$, (b) $p=0.27$, (c) $p=0.3$, (d) $p=0.5$, (e) $p=1.0$.
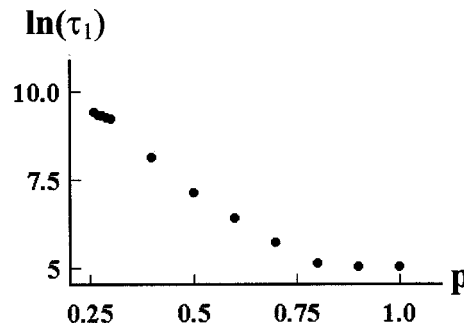

FIG. 7. Effective relaxation time τ for the dispersion of the effective conductivity $\sigma_e \propto \omega^\alpha$ obtained from computer simulations as a function of the concentration of the conducting bonds p.
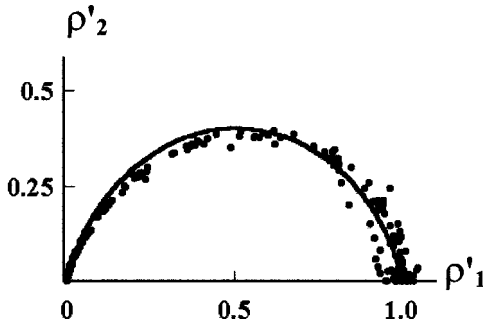
FIG. 8. Nyquist plot of the reduced resistivity ρ'. Computer data collapse on the single curve obtained from Eq. (30), which gives essentially the same Nyquist plot for all concentrations p.

slope of $\sigma_1(\omega)$ in Fig. 4. There are two exponents α_1 and α to describe the dispersion for the frequencies $\omega \propto 1/\tau_1$ and $\omega \propto 1/\tau$, respectively. The exponent α is nonuniversal.

B. Frequency dependence of the impedance in vicinity to percolation threshold

Let us now start the interpretation of the numerical results. For different phenomena, we can define different correlation lengths. If the size of the system is large compared to this specific correlation length, the system can be considered as homogeneous for this phenomenon.

To understand the behavior of the effective complex conductivity $\sigma_e(p,\omega')$ in the considered system, it is instructive to start with concentration p close to the percolation threshold p_c. At this concentration, the backbone of the infinite cluster of the conducting channels can be viewed as a Skal–Shklovskii–De Gennes superlattice[15] consisting of nodes connecting via macrobonds. The macrobonds have self-similar blobs—link structures such as that shown in Fig. 3. Macrobonds necessarily include single connected parts—red bonds. The geometrical distance between neighboring nodes in the Skal–Shklovskii–De Gennes superlattice is the percolation correlation length $\xi_p \cong a_0(p-p_c)^{-\nu}$, where a_0 is the microscopical scale for the problem (e.g., the average size of brushite grains) and critical exponent ν is equal to $\nu \cong 0.88$ for 3D systems.[15] From now on we will measure all the distances in terms of a_0 (i.e., put $a_0=1$). The length L_s of the shortest path between two nodes in the superlattice is certainly larger than the geometrical distance ξ_p between them. The following equation holds for this length $L_s \cong \xi_p^{\eta_s}$, where the critical exponent $\eta_s > 1$ (Refs. 15, 31, and 32). If only the red bonds are taken into account, the critical exponent η_s is equal to $\eta_s = 1/\nu \approx 1.14$ (Refs. 15, 31, and 32), that is, the length of a macrobond in the superlattice is much larger than the geometrical distances between its ends $L_s/\xi_p \to \infty$ for concentrations $p \to p_c$. For a percolating system with identical conducting elements the conductance of a macrobond between two nodes in the Skal–Shklovskii–De Gennes superlattice $\sigma(L_s)$ can be estimated as $\sigma(L_s) \cong \sigma_0/L_s$, where σ_0 is the conductivity of the conducting element. A percolating system is considered homogeneous for scales larger than the correlation length ξ_p. Therefore, the effective conductivity σ_e is estimates to be

$$\sigma_e \cong \sigma(L_s)/\xi_p = \sigma_0 \xi_p^{-(1+\eta_s)} \cong \sigma_0(p-p_c)^t, \quad (14)$$

where the critical exponent $t = \nu + \eta_s \nu$. So, if we take into account only the red bonds and identical conducting bonds, the critical exponent is $t = \nu + 1 \cong 1.88$.[15] This value of the exponent t is not far away from the value $t \cong 2.05$ calculated above.

Now, let us take into account the distribution of the conducting bonds given by Eq. (5). We still calculate near the percolation threshold p_c. We also assume that the dimensionless frequency ω' in Eq. (5) is small enough [$\omega' \leq \exp(-\lambda)$]. From now on we take $\sigma_0=1$. To find the conductance of a macrobond in a Skal–Shklovskii–De Gennes superlattice we follow the procedure outlined in Ref. 33. Let us consider a macrobond which connects two nodes separated by the distance ξ_p. We first "switch off" all elementary conducting bonds in the macrobond. Then we restore the elementary bonds in the macrobond starting with the one having the largest modulus of conductivity. We continue the procedure until a conducting path spans between the two ends of the macrobond. The smallest conductivities included in this first conducting path have value $\sigma_c = -i\omega' + \exp(-\lambda x_c)$, where the concentration x_c is equal to the percolation threshold $x_c = p_c/p$ for the percolating problem that is set by the backbone itself.[15,26,31] The conductance of the macrobond is determined by the conductance of the first path since all other bonds that are inserted afterwards have smaller conductivities in absolute value than σ_c. That is, we suppose that the electric current chooses a single path consisting of bonds with the largest conductivities in any blob of the backbone. In analogy to the well-known relation $L_s \cong \xi_p^{\eta_s}$, it is natural to suppose that length L of the first conducting path also has a scaling dependence on the correlation length, i.e., $L \propto \xi_p^\eta$. This new critical exponent η is, in general, larger than the critical exponent for the shortest path $\eta \geq \eta_s$, since the first conducting path consists of the bonds which have the largest conductivities. These bonds do not necessarily coincide with those in the shortest path between two nodes in the superlattice. The value of the exponent η will be determined below. Since the first conductance path consists of bonds connected in series, its conductance $\sigma(L)$ can be estimated as $\sigma(L) = (\langle \rho \rangle_c L)^{-1}$, where $\langle \rho \rangle_c$ is the average complex resistivity of the bonds belonging to the path. The conductivities of the bonds in the first path are still distributed according to Eq. (5), but the random variables x_i are now in the range $0 < x_i < p_c/p$. The average of the bond resistivity $\rho_i = 1/\sigma_i = [-i\omega' + \exp(-\lambda x_i)]^{-1}$ is then obtained as

$$\langle \rho \rangle_c = \int_0^{p_c/p} [-i\omega' + \exp(-\lambda x)]^{-1} dx$$

$$\cong \frac{ip}{p_c \lambda \omega'} \ln\left(\frac{1 - i\omega' \exp[\lambda(p_c/p)]}{1 - i\omega'}\right). \quad (15)$$

From this equation, it follows that the effective complex conductivity $\sigma_e^a \propto \sigma(L)/\xi_p = (\langle \rho \rangle_c L \xi_p)^{-1}$ of the percolating system with exponentially distributed conductivities and concentrations p close to p_c is equal to

$$\sigma_e^a(p,\omega') = A \frac{\lambda p_c}{p} \frac{-i\omega'(p-p_c)^{(1+\eta)\nu}}{\ln(\{1 - i\omega' \exp[\lambda(p_c/p)]\}/(1 - i\omega'))}, \quad (16)$$

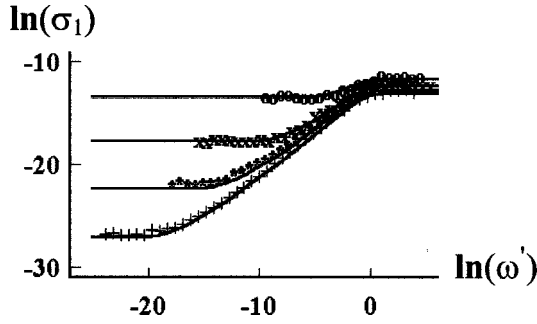FIG. 9. Real part of the effective conductivity σ_1 obtained from computer simulations exactly at the percolation threshold as a function of reduced frequency ω' for different values of parameter λ: $+: \lambda=20, *: \lambda=15, \times: \lambda=10.0, \bigcirc: \lambda=5.0$.

where A is some numerical coefficient. Remember that we have taken $\sigma_0=1$. When frequency goes to zero the effective conductivity approaches the static limit

$$\sigma_e^a(p)=A\,\frac{\lambda p_c}{p}\,(p-p_c)^{(1+\eta)\nu}\exp[-\lambda(p_c/p)], \quad (17)$$

where the concentration of the conducting component p is still supposed to be close to the percolation threshold p_c.

C. Scaling consideration at the percolation threshold

Exactly at the percolation threshold $p=p_c$, we should substitute the system size L to the correlation length ξ_p in the equation $\sigma_e\propto(\langle\rho\rangle_c L\xi_p)^{-1}$ according to the finite size arguments.[15] Then Eq. (16) takes the following form:

$$\sigma_e(L,\omega')\propto\frac{-i\omega'\lambda L^{-(1+\eta)}}{\ln\{[1-i\omega\,\exp(\lambda)]/(1-i\omega')\}}, \quad (18)$$

Using the ENR method, we have calculated the static conductivity $\sigma_e(L)=\sigma_e(L,0)$ at the percolation threshold for different values of the system size L and for different parameters λ. The static conductivity $\sigma_e(L)$ appears to agree best with the equation $\sigma_e(L)\cong\lambda\,\exp(-\lambda)/L^{1+\eta}$, which follows from Eq. (18) in the limit $\omega'\to0$. From these calculations, we estimate that critical exponent η is equal to $\eta=1.5\pm0.1$.

In Fig. 9, we present the effective conductivity $\sigma_e(\omega')$ calculated at the percolation threshold for the fixed $L=64$ and different values of the reduced frequency ω' and parameter λ. We can see that the obtained effective conductivity follows Eq. (18) for the entire frequency range even though Eq. (18) was obtained for $\omega'<\exp(-\lambda)$ only. This means that the same path gives the most important contribution to the conductance of a macrobond no matter what the value of the frequency is. If we adopt this suggestion, we can estimate the critical exponent t to be $t=\nu(1+\eta)\approx2.2$ which agrees with the result of Sec. III.

Since Eq. (18) fits the computer data very well, we use this equation to calculate the exponent α: $\alpha=\max_{\omega'}\{\partial\ln[\sigma(\omega')]/\partial\ln(\omega')\}$. We solve equation $\partial^2\ln[\sigma(\omega')]/\partial\ln(\omega')^2=0$ numerically and obtain that the maximum is achieved at frequency ω'_α, which can be approximated with very good accuracy as
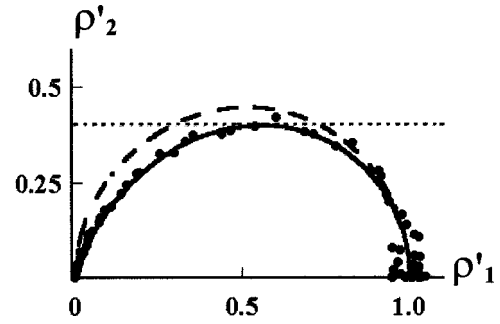

FIG. 10. Nyquist plot of the reduced resistivity ρ' obtained exactly at the percolation threshold. The points for $\lambda=20, 15, 10.0, 5.0$ collapse on the single curve that is given by Eq. (18) and are independent of parameter λ for $\lambda>4$. The dashed line is Nyquist plot from Eq. (18) for $\lambda=2$. The dotted line is the universal value of damping parameter $\beta=\ln\frac52$.

$$\omega'_\alpha\approx\exp[-\lambda/2\ln(\lambda)], \quad \lambda\gg1. \quad (19)$$

We can introduce the relaxation time $\tau=1/\omega'_\alpha$ which corresponds to the power-law dispersion of the complex impedance $Z(\omega')\propto(\omega')^\alpha$. Substituting ω'_α given by Eq. (19) in the expression for the exponent $\alpha=\{\partial\ln[\sigma(\omega')]/\partial\ln(\omega')\}_{\omega'=\omega'_\alpha}$ we obtain the following equation:

$$\alpha=1-\frac{4\lambda}{\lambda^2+\pi^2}, \quad \lambda\gg1, \quad (20)$$

which actually stands for all parameters $\lambda>1$. Equation (20) gives $\alpha=0.64$ for $\lambda=10$ in good agreement with the results of our computer simulation for concentrations p close to the percolation threshold p_c (see Fig. 6). It follows from Eq. (20) that the exponent α achieves its asymptotic value $\alpha=1$ for $\lambda\to\infty$; this value can only be considered as universal (which means that it is independent of the particular features of the system) when the parameter λ becomes very large.

Consider now the Nyquist plots of the reduced complex resistivity $\rho'(L,\omega')=\rho'_1(L,\omega')+i\rho'_2(L,\omega')=\sigma(L,0)/\sigma(L,\omega')$ calculated using the ENR procedure for $p=p_c$. They are presented on Fig. 10 together with the curve obtained from Eq. (18). We observe that all data are superimposed on the curve fitted by Eq. (18). The damping parameter is equal to $\beta=\max[\rho'_2(L,\omega')]_{\omega'}/\rho'_1(L,\omega'\to0)\cong0.41$ for the curve in Fig. 10 and exponent α_1 in Eq. (13) is then equal to $\alpha_1=0.86$. The imaginary part of the reduced resistivity $\rho'_2(\omega)$ is a maximum for the frequency $\omega'_0=1/\tau_1$. From analysis of Eq. (18), we obtain in the limit $\lambda\gg1$:

$$\omega'_0\approx\{A+O[\exp(-\lambda)]\}\exp(-\lambda), \quad A=1.980\,29\ldots\approx2, \quad (21)$$

where A is the solution of the equation $2A^2/(1+A^2)-\ln(1+A^2)=0$. Substituting $\omega'_0\approx2.0\exp(-\lambda)$ back into Eq. (18), we obtain the following expression for the damping parameter β as a function of the disorder parameter λ:

$$\beta\cong\frac{1}{4(1-e^{-\lambda})}\ln\left(\frac{5}{1+4e^{-2\lambda}}\right), \quad \lambda\gg1. \quad (22)$$

It follows from these equations that the damping parameter β achieves its asymptotic value $\beta = \ln(5)/4 \approx 0.4$ very rapidly with increasing parameter λ. The exponent $\alpha_1 = (4/\pi)\arctan(2\beta)$ reaches its asymptotic value

$$\alpha_1 = \frac{4}{\pi} \arctan\left(\frac{\ln 5}{2}\right) \cong 0.86 \qquad (23)$$

already at $\lambda \geq 4$. Thus, it is not surprising that the computer data are all on a single curve in Figs. 8 and 10. Again, the asymptotic value of the exponent α_1 can be considered as ''universal'' as soon as the disorder is large enough.

It follows from the above consideration that there are two characteristic time scales in the system $\tau \cong \exp(\lambda/2 \ln \lambda)$ and $\tau_1 \cong \exp \lambda/2 \gg \tau$, given by Eqs. (19) and (20), correspondingly. The frequency dependence of the complex impedance $Z(\omega')$ is quite different in these two scales. For the frequencies $\omega' \propto 1/\tau$, it is power-law dispersion $Z_1 \propto Z_2 \propto {\omega'}^\alpha$ while for $\omega' \propto 1/\tau_1$ imaginary part of the impedance $Z_2(\omega')$ reaches a maximum at the frequency $\omega' = 1/\tau_1$ and the whole dispersion behavior can be imaged as a depressed semicircle in the $\{Z_1, Z_2\}$ Nyquist plot. It is worth noting that system behavior becomes universal for *both* time scales when the disorder in the system increases.

For small values of the parameter λ (ordered systems or rather large temperature), Eq. (22) gives the damping parameter β in the following form:

$$\beta \cong \frac{1}{2} - \frac{\lambda^2}{48}, \quad \lambda < 1, \qquad (24)$$

which gives the damping parameter $\beta = \frac{1}{2}$ for $\lambda = 0$, i.e., when all conducting elements have the same conductivity so that the dispersion behavior of the complex resistivity reduces to simple Debye relaxation. Indeed, for $\beta = \frac{1}{2}$ we obtain $\alpha_1 = 1$. In Fig. 10 we show the Nyquist plot of the reduced resistivity $\rho'(\omega')$ obtained from Eq. (18) for an intermediate case, namely, for $\lambda = 2$. The corresponding curve goes somewhat higher than the curves for the larger values of the parameter λ and is a less depressed semicircle.

It follows from Eqs. (20) and (22) that exponents α and α_1 obtained from the $\sigma(\omega')$ dependence and the Nyquist plot, correspondingly, are not independent. The exact forms of Eqs. (20) and (22) have been obtained for systems at the percolation threshold. Let us suppose for a moment that Eqs. (20) and (22) can be applied not only for the system at the percolation threshold $p = p_c$ but for all concentration p. We have defined the effective relaxation time τ_1 as the inverse of the characteristic frequency $\omega_0'(p)$ corresponding to the maximum of the imaginary part ρ_2' of the complex resistivity $\tau_1(p) = 1/\omega_0'(p)$. On the other hand Eq. (21) gives $\omega_0'(p_c) = 1/\tau_1(p_c) = 2 \exp(-\lambda)$. We can define the effective parameter λ_e for the entire concentration range from the equation $1/\tau_1(p) = 2 \exp[-\lambda_e(p)]$, which gives $\lambda_e(p) = -\ln[2\tau_1(p)]$. Substituting the thus defined effective parameter $\lambda_e(p)$ in Eq. (20), we obtain the following equation:

$$\alpha(p) = 1 - \frac{4 \ln[2\tau_1(p)]}{\ln^2[2\tau_1(p)] + \pi^2}, \qquad (25)$$

which connects the exponent α and the effective relaxation time $\tau_1(p)$ for any arbitrary concentration $p \geq p_c$. We take

the previously determined effective relaxation times (see Fig. 7) and substitute them in Eq. (25). The obtained ''theoretical'' values for the exponent $\alpha(p)$ are shown in Fig. 6 by squares. There is rather good agreement between the exponent α originated directly from the computer simulations and that from Eq. (25). This would mean that Eqs. (19)–(25) can be applied to any inhomogeneous system with exponentially distributed local conductivities as soon as the notion of local conductivity can be introduced. The effective relaxation time τ_1 has been obtained from a Nyquist plot whereas the exponent α determines the power-law behavior of the effective conductivity $\sigma_e(\omega) = 1/\rho_e(\omega) \propto \omega^\alpha$ for frequencies much larger than $1/\tau_1$ [cf. Eqs. (19) and (21) for $\lambda \gg 1$]. Still these quantities appear to be connected to damping parameter β as well.

D. Scaling equation for the complex impedance in the entire concentration range

We return now to our system analysis for an arbitrary concentration p of the conducting bonds. As one might expect, the static conductivity $\sigma_e^a(p)$ given by Eq. (17) is determined by the smallest critical conductivity $\sigma_c \cong \exp[-\lambda(p_c/p)]$ obtained from the first conducting path through a macrobond. The conductivities in the first conducting path are distributed by Eq. (5) where the random variables x_i take values in the interval $0 < x_i < p_c/p$. Then the length ℓ of the segments of the conducting path between two critical conductivities can be estimated as $\ell \propto \lambda p_c/p$. Therefore, the above considerations of the percolating system with exponentially distributed conductivities hold when the length of the first conducting path $L \propto \xi_p^\eta$ is much larger than the length ℓ, this means that the percolation correlation length must be large enough: $\xi_p \gg [\lambda(p_c/p)]^{1/\eta}$.

We turn now to the opposite case, namely, we consider concentrations p of the conducting bonds such that the percolation correlation length is relatively small $\xi_p \ll [\lambda(p_c/p)]^{1/\eta}$, but still $\xi_p \gg 1$. Recall that we are interested in systems with parameter $\lambda \gg 1$. Let us start with small frequencies $\omega' < \exp(-\lambda)$. To estimate the effective conductivity $\sigma_e(p,\omega')$ we consider a system with size $L \gg [\lambda(p_c/p)]^{1/\eta} \gg \xi_p$. We again switch off all the conducting bonds in the system and then restore them starting with the largest modulus of the conductivity σ_i in order of decreasing values. Suppose that we restore the x part of the conducting bonds to its original form, therefore we restore the bonds with conductivities $|-i\omega' + \exp(-\lambda x)| < |\sigma_i| < |-i\omega' + 1|$. At concentration $x = x_c$ the first conducting path spans the system. The volume concentration of the restored bonds is equal to xp, therefore the critical concentration x_c is equal to $x_c = p_c/p$.[15,19,34] The resistance of the first conducting path is estimated to be that for a macrobond [see discussion after Eq. (14)]. Therefore, the path resistance is proportional to $\langle\rho\rangle_c L^\eta$, where $\langle\rho\rangle_c$ is given by Eq. (15), and L^η is the effective length of the path. Then the conductivity of the whole system is estimated to be

$$\sigma_e(x_c) \cong \frac{1}{\langle\rho\rangle_c L^{1+\eta}}, \qquad (26)$$

where the average resistivity $\langle\rho\rangle_c$ is still given by Eq. (15). When we restore more and more bonds, they form the Skal–

Shklovskii–De Gennes superlattice. The period of the super-lattice period ξ_x decreases as the concentration x of the restored conducting bonds increases. The effective conductivity $\sigma_e(x) \cong 1/(\langle\rho\rangle_c \xi_x^{1+\eta})$ increases with decreasing ξ_x until the characteristic size

$$\xi_c \cong (\lambda x_c)^{1/\eta} \gg \xi_p \qquad (27)$$

is reached. This new characteristic length is related to current inhomogeneities. The conductance of a macrobond with size $\xi_x \cong \xi_c$ can be estimated as $\sigma_c \cong 1/(\langle\rho\rangle_c \xi_x^\eta) \cong 1/(\langle\rho\rangle_c \lambda x_c) \sim \exp(-\lambda x_c)$. If we go on restoring the conducting bonds, i.e., switch on the bonds with conductivities $|\sigma_i| < \exp(-\lambda x_c)$, the effective conductivity will not change since the new bonds have conductances smaller than the macrobond conductance σ_c. Therefore, the effective conductivity for the concentrations p corresponding to the correlation length $\xi_p < \xi_c$ can be obtained from Eq. (16) if we substitute the conductivity correlation length $\xi_c \cong (\lambda x_c)^{1/\eta}$ to the percolation correlation length $\xi_p \propto (p - p_c)^{-\nu}$. Thus, we obtain the following equation for the effective conductivity $\sigma_e^b(p, \omega')$ in the concentration range corresponding to the condition $\xi_p < \xi_c$:

$$\sigma_e^b(p,\omega') = B\left(\frac{p}{\lambda p_c}\right)^{1/\eta} \frac{-i\omega'}{\ln\left(\frac{\{1 - i\omega'\exp[\lambda(p_c/p)]\}}{(1 - i\omega')}\right)}, \qquad (28)$$

where B is another numerical factor.

In the limit $p = 1$ and $\omega' = 0$ the effective conductivity given by Eq. (28) becomes $\sigma_e(1,0) \propto \exp(-\lambda p_c)/(\lambda p_c)^{1/\eta}$ ($\lambda \gg 1$), which is similar to the well-known result $\sigma_e \propto \exp(-\lambda p_c)/(\lambda p_c)^\nu$ for the static conductivity of a regular lattice with exponentially distributed bond conductivities.[33] However, in the earlier works[33] only the red bonds in a macro-bond were considered, whereas we now take into account the whole blob-link structure of the backbone. Consequently, we obtain a new critical exponent $1/\eta$ instead of the exponent ν for the percolation correlation length. It is not surprising that Eq. (28) derived originally for concentrations close to the percolation threshold gives exact results for $p = 1$. The geometry of the percolating system is essentially the same for both limiting cases since the system can be viewed as a regular lattice of the conducting bonds. The only difference is that for $p = 1$ the period of the lattice is equal to a microscopical scale a_0 while for $p \to p_c$ it is equal to the percolation correlation length ξ_p. Nevertheless, this difference is inessential as soon as the current inhomogeneity scale ξ_c is larger than the scale of geometric inhomogeneity $\xi_c > \xi_p$.

The effective conductivities σ_e^a and σ_e^b, given by Eqs. (16) and (28), respectively, have the same form at concentration p^*, corresponding to the condition $\xi_p = \xi_c$. That is, where the scale for the geometric inhomogeneity ξ_p is equal to the scale of the electric current inhomogeneity ξ_c. To calculate the effective conductivity σ_e in the entire region of the concentration we use the simplest interpolation equation $\sigma_e = (\sigma_e^a \xi_p^{1+\eta} + \sigma_e^b \xi_c^{1+\eta})/(\xi_p^{1+\eta} + \xi_c^{1+\eta})$, which takes the form

$$\sigma_e(p,\omega') = \frac{-ip_c\lambda\omega'}{p\,\ln(\{1 - i\omega'\exp[\lambda(p_c/p)]\}/(1 - i\omega'))[(p - p_c)^{-(1+\eta)\nu}/A + (\lambda p_c/p)^{1+1/\eta}/B]}, \qquad (29)$$

where A and B are numerical factors that appeared before in Eqs. (16) and (28), respectively.

We show in Fig. 11 the effective static conductivity $\sigma_e(p,0)$ given by Eq. (29) together with results of the computer simulations. The factors A and B have been chosen to be equal to $A = 0.035$ and $B = 2.1$, respectively. There is good agreement between computer data and the results of interpolated Eq. (29). Note that there is no concentration range in Fig. 11 where the conductivity is linear with respect to the concentration p, as predicted by perturbation theory[35] and effective medium theories.[15] Instead, the behavior of the static conductivity σ_e looks similar to scaling law $\sigma_e \propto (p - p_c)^t$ with the exponent t about $t \cong 2$ in the entire range of the concentration. This result can be understood if we recall that the spatial scale of the current inhomogeneity $\xi = \max\{\xi_p, \xi_c\}$ is larger than microscopical scale a_0 for all concentrations p in the considered percolating system with exponentially distributed local conductivities.

We showed above that Eq. (16) (concentration range such that $\xi_p > \xi_c$) describes the results of the computer simulations well for the entire range of frequency ω. Equation (28) (condition $\xi_p < \xi_c$) was originally derived for the reduced frequency $\omega' < \exp(-\lambda)$. It is easy to show that it can be

used for a much wider frequency range, namely, for $\omega' < \exp(-\lambda p_c/p)$. Indeed, the derivation of Eq. (28) is based on the separation of the conducting bond of those with conductivities $|\sigma_i| \equiv |-i\omega' + \exp(-\lambda x_i)| \geq \sigma_c$ and $|\sigma_i| \equiv |-i\omega' + \exp(-\lambda x_i)| < \sigma_c$, where the critical conductivity σ_c is equal to $\sigma_c = \exp(-\lambda p_c/p)$. It was shown that conducting bonds with $|\sigma_i| \geq \sigma_c$ are responsible for the effective conduc-
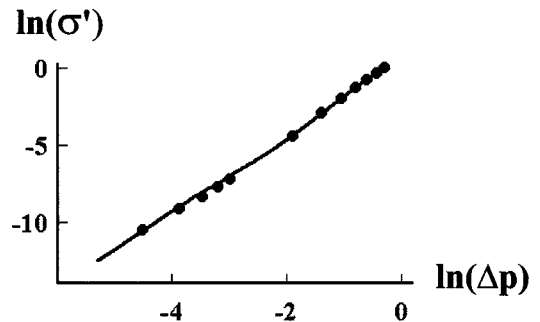

FIG. 11. Effective static conductivity of the percolating system with exponentially distributed local conductivity. ●: computer simulations, the line is the static conductivity given by Eq. (29) for $\lambda = 10$, $\omega = 0$, $A = 0.035$, $B = 2.1$.

tivity of the system. If the frequency is such that $\omega' < \sigma_c$, the above separation does not change and, therefore, there is no effect on the derivation of Eqs. (28) and (29).

To find the effective conductivity for larger frequencies ($\omega' > \sigma_c$) let us consider again a system with size $L \gg \xi_c \gg \xi_p$. The number of conducting channels N_p which span the system from, say, top to bottom, can be estimated as $N_p \propto (L/\xi_p)^2$. For $\omega' < \sigma_c$, only $N_c \propto (L/\xi_c)^2 \ll N_p$ channels have conductivities $|\sigma_i| \gtrsim \sigma_c$ which are responsible for the effective conductivity. Their contribution to the conductance Σ of the system is estimated as $\Sigma_c \cong L/(\xi_c^{1+\eta}\langle\rho\rangle_c)$, where $\langle\rho\rangle_c$ is given by Eq. (15). The other $N_p - N_c \approx N_p$ channels contain nearly *all* conductivities and, therefore, their contribution to the conductance Σ can be written as $\Sigma_p = N_p/(L\xi_p^{\eta+1}\langle\rho\rangle) \cong L/(\xi_p^{\eta+1}\langle\rho\rangle)$, where $\langle\rho\rangle$ is the bond resistivity averaged on all channels. However, this conductance Σ_p becomes important when the frequency increases,

$\omega > \sigma_c$. Therefore, the term $\sigma_e^c = \Sigma_p/L \propto (\xi_p^{\eta+1}\langle\rho\rangle)^{-1}$ should be added to Eq. (28) for the effective conductivity σ_e^b to extend this equation for the entire frequency range. We can also add the same term to the effective conductivity σ_e^a given by Eq. (16), which holds for $\xi_p \gg \xi_c$, i.e., for concentrations p near the percolation threshold p_c. Indeed, the conductivity σ_e^c resembles the conductivity σ_e^a for $p \to p_c$ and the addition of σ_e^c to Eq. (16) just leads to some renormalization of the numerical factor A.

From the above discussion, it follows that we just have to add the conductivity σ_e^c to the interpolating equation (29) to extend its application to the entire frequency range. Thus, we obtain the following equation for the effective complex conductivity [recall that all conductivities and frequencies are measured in terms of the conductivity σ_0 appearing in Eq. (4)]

$$\sigma_e(p,\omega') = \frac{-ip_c\lambda\omega'}{p\,\ln(\{1-i\omega'\,\exp[\lambda(p_c/p)]\}/(1-i\omega'))[(p-p_c)^{-(1+\eta)\nu}/A + (\lambda p_c/p)^{1+1/\eta}/B]}$$
$$+ \frac{-i\lambda\omega'}{\ln\{[1-i\omega'\,\exp(\lambda)]/(1-i\omega')\}}\left(\frac{p-p_c}{1-p_c}\right)^{(1+\eta)\nu}\left(1 - \frac{(\lambda p_c)^{-(1+1/\eta)}}{B}\right), \tag{30}$$

where p is the volume concentration of the conducting component in the percolating system (e.g., brushite grains), p_c is the actual percolation threshold in the considered system, $\omega' = \omega/(4\pi\sigma_0)$ is the reduced frequency of the external ac field, λ and σ_0 are parameters of the exponential distribution of the local conductivities in the system [see Eq. (4), parameter $\lambda \gg 1$], $\eta \cong 1.5$ is the critical exponent found in the present work, $\nu \cong 0.88$ is the critical exponent for the percolation correlation length, and $A = 0.035$ and $B = 2.1$ are numerical coefficients. The numerical coefficient in the last term of Eq. (30) has been chosen so that the effective conductivity $\sigma_e(p,\omega')$ resembles the exact result $\sigma_e(1,\omega' \to \infty) \cong -i\omega'$, which holds for the considered system. A scaling equation of the form of Eq. (30) can be used to estimate complex impedance of any physical system with exponentially distributed local conductivities.

However, we should note that Eq. (30) was obtained in a somewhat rough approximation since all the elements of the system which are not included in the Abraham-Miller network are assumed to be connected in series. On the other hand, it is well known that resistive elements that are not incorporated in the backbone for the most part in series with the C elements in usual R-C percolating systems. We will show that the assumptions made in order to obtain Eq. (30) from Eq. (29) prove themselves in practical calculations. The precise description of the complex effective conductivity of a percolating system with an exponentially wide distributed real part of the local conductivity deserves further consideration.

Figures 4, 5, and 8 show that Eq. (30) reproduces the numerical results of the computer simulation in the entire concentration and frequency range. The resemblance cannot

be coincidental. Let us stress again that the existence of an analytical equation which is valid for the entire concentration region ($p_c \leq p \leq 1$) and all frequencies is accounted for by the current and field inhomogeneity scale and far exceeds the microscopical scale a_0. Moreover, the inhomogeneity scale is large as compared to a_0 for all concentrations and for almost all frequencies. Note that agreement between computer data and the theory is somehow inferior for $\omega' \to \infty$ when the inhomogeneity scale shrinks to the microscopical scale a_0.

V. EXPERIMENTAL RESULTS AND COMPARISON WITH THE THEORY

A. Dry brushite composites

The brushite composite samples used for measurements are pellets, 20 mm in diameter and 1–3 mm in thickness. They were pressed at 1.6 kbar for 20 min and are composed of two mixed powders of brushite and polymer (polyphenylsulfur). The average size of the brushite and polymer grains is 18 μm and 42 μm, respectively. For electric measurement, we use an EGG device (model 273A) coupled with a Schlumberger 1255 SI locked-in amplifier. The electrodes are gold and the frequency range for the measurements of the complex impedance $Z(\omega)$ is $[10^{-1}$ Hz,10^4 Hz$]$. The details of the experimental procedure can be found elsewhere.[8]

The brushite powder was first dried in an oven. Immediately after compacting, the samples have no dc conductivity; they behave as insulators. After being stored for a few days at room atmosphere, they acquire a well-defined conductivity, as reported below, which does not change during the process of measurement. We will refer to this set of samples
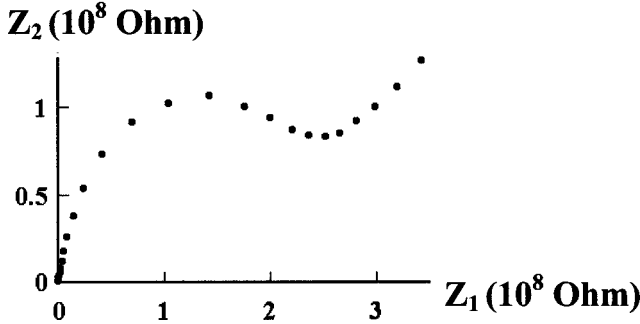
FIG. 12. Nyquist plot of the complex impedance $Z(\omega)$ $= Z_1(\omega) + iZ_2(\omega)$ for the brushite composite with concentration p $= 0.4$.
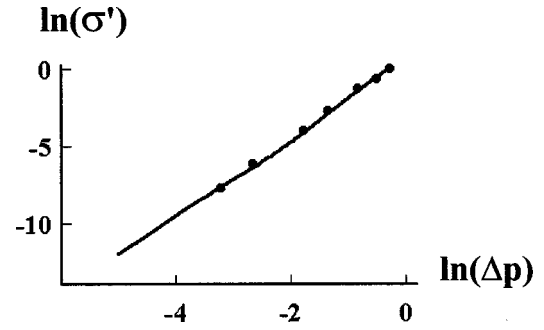

FIG. 13. Effective static conductivity of the percolating system with exponentially distributed local conductivity. ●: dry brushite composites, line is given by Eq. (29) for different $\Delta p = p - p_c$ and for $\lambda = 10.1$, $\omega = 0$, $A = 0.035$, $B = 2.1$.

as dry samples, and most of the experimental results presented here were obtained from these samples. To verify the suggestion that the finite conductivity can be attributed to a thin layer of absorbed water on the brushite grains we have prepared another series of composites—wet samples. The wet samples were prepared in the same conditions, but with a brushite powder kept in a water saturated enclosure for 48 h before compacting. Thus, the obtained wet composites have a dc conductivity of about two orders of magnitude larger than that of the dry samples.[8–10]

The volume concentration p of the brushite grains and pores is equal to $p = 1.0$, 0.84, 0.67, 0.49, 0.4, 0.3, and 0.27 for the dry samples. The Nyquist plot of the complex impedance $Z(\omega) = Z_1(\omega) + iZ_2(\omega)$ of a sample with brushite concentration $p = 0.40$ is shown in Fig. 12. We can observe a depressed semicircle that is completed by an increase of both $Z_1(\omega)$ and $Z_2(\omega)$ parts of the impedance $Z(\omega)$ at small frequencies (right part of Fig. 12). Such a Nyquist plot is typical for many inhomogeneous ionic conductors (see, e.g., Refs. 1–5). It is commonly accepted that the increase of $Z_1(\omega)$ and $Z_2(\omega)$ at low frequencies is due to processes at the electrodes (Warburg impedance behavior, discussed at the end of Sec. II). We are not interested in electrode processes in this paper and will, from now on, omit the low frequency points and only keep higher frequencies where the Nyquist plots for our samples have a well-developed semicircle shape.

We extrapolate the semicircle impedance data to obtain the static conductivity of the brushite composites themselves, apart from electrode effects. Two methods for the extrapolation have been used: direct extrapolation and the fitting of a Nyquist plot by empirical equation (1). Both methods give essentially the same results shown in Fig. 13 where we plot reduced static conductivity $\sigma'(p) = \sigma(p)/\sigma(1)$ as a function of $\Delta p = p - p_c$. We chose for this series of samples the percolation threshold $p_c = 0.23$. It is not surprising that the static conductivity in Fig. 13 follows the power-law behavior $\sigma' \propto (\Delta p)^t$ for concentrations close to the percolation threshold. What may be more surprising is that the critical behavior $\sigma' \propto (\Delta p)^t$ starts at $p = 1$ and holds in the *entire* concentration range. To understand the origin of the concentration variation of the static conductivity, we fit the experimental data by Eq. (29) obtained in the previous section for a percolating system with exponentially distributed local conductivities. We put the numerical coefficients A and B in Eq.

(29) to be the same as those we used to describe the computer data (see Fig. 11). Therefore we are left with only one fitting parameter λ which is found to be $\lambda = 10.1$. Then Eq. (29) exactly reproduces the experimental results for the reduced static conductivity $\sigma'(p)$. This allows us to assume that in the static case the contact conductivities σ_i between the brushite grains are distributed exponentially $\sigma_i \propto \sigma_0 \exp(-\lambda x_i)$, where $\lambda = 10.1$, and the random variables x_i take values $0 < x_i < 1$ [see Eq. (4)]. The prefactor σ_0 can be estimated from the experimental value $\sigma(1) = 1.1 \times 10^4$ sec^{-1} [$1.3 \times 10^{-8}(\Omega$ cm$^{-1})$] and Eq. (29) to be equal to $\sigma_0 = 4.1 \times 10^5$ sec^{-1}. For the exponential distributed local conductivities, the spatial scale for the electric current inhomogeneity exceeds the microscopical scale in the problem, namely, the average size of the brushite grains, significantly for all concentrations p. Consequently, we obtain a ''scaling'' behavior of the static conductivity, as a function of p, for the entire concentration range from $p = 1$ until the percolation threshold $p = p_c$.

The Nyquist plots of the reduced complex impedance $\rho'(\omega) = \rho_1'(\omega) + i\rho_2'(\omega) = Z(\omega)/Z(0)$ are shown in Fig. 14 for all values of the concentration p. We have omitted the low frequency experimental points (right part of the Nyquist plot), which are related to the Warburg impedance behavior. All other experimental points are situated on a single depressed semicircle, which is well reproduced by Eq. (30). We still use parameters $A = 0.035$ and $B = 2.1$ which were the
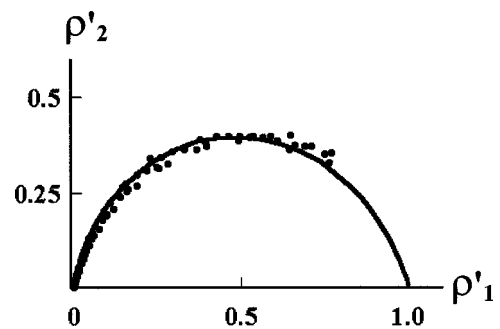

FIG. 14. Nyquist plot of the reduced resistivity ρ'. Experimental data for the brushite composites collapse on the single curve obtained from Eq. (30), which gives essentially the same Nyquist plot for all concentrations p. The parameters in Eq. (30) are $\lambda = 10.1$, $\omega = 0$, $A = 0.035$, $B = 2.1$.
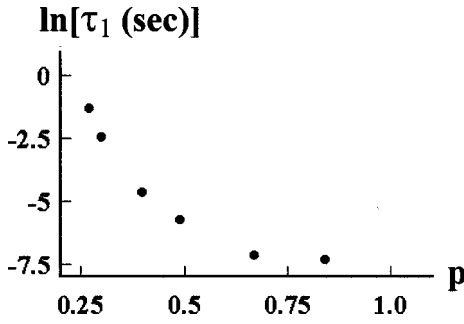
FIG. 15. Effective relaxation time τ_1 for brushite composites as a function of the concentration p. Relaxation time τ_1 is obtained as $\tau_1 = 1/\omega_0$, where the frequency ω_0 corresponds to the maximum of the imaginary part of the resistivity $\rho_2'(\omega)$.

FIG. 16. Real part of the effective conductivity σ_1 for brushite composites as a function of the frequency ω; different series of experimental points correspond to different concentrations: (a) $p = 0.27$, (b) $p = 0.3$, (c) $p = 0.4$.

best found for the computer data in Sec. IV. The parameter $\lambda = 10.1$ was determined above from the concentration dependence of the static conductivity. Note that Eq. (30) is written for the dimensionless frequency ω'. To find the actual dependence of the effective conductivity (resistivity) on the frequency it is necessary to introduce the *corresponding characteristic frequency* ω^* in Eq. (30). Below, we determine the characteristic frequency ω^* for this series of samples. However, as soon as we have only one depressed semicircle in the Nyquist plot, the shape of the plot does not depend on the characteristic frequency. A change in ω^* causes the points to move along the curve only. Therefore, we use Eq. (30) as it is and obtain that all experimental points collapse on the theoretical curve. Figure 14 shows that the damping parameter $\beta = \max[\rho_2'(\omega)]$ is essentially the same for all concentrations p being studied in the experiment. The experimental value of the parameter $\beta \approx 0.4$ corresponds to the ''universal'' value $\beta = \ln(5)/4$ which we propose for systems with exponentially distributed local conductivities.

We can define the effective relaxation time τ_1 for the complex impedance or conductivity as $\tau_1 = 1/\omega_0$, where ω_0 is the frequency wherein the imaginary part $\rho_2'(\omega)$ is a maximum. This definition of the relaxation time agrees with the empirical equation (13) often used for fitting experimental data.[1–5] The defined relaxation time τ_1 is shown in Fig. 15 for different concentrations p. We observe that τ_1 increases by several orders of magnitude as the concentration p decreases towards the percolation threshold. This behavior of the relaxation time τ_1 is similar to the one obtained in the computer simulations (see Fig. 7) and can be explained in the following way. All contacts between the grains that are essential for the effective conductivity are connected in series for the concentrations of the conducting component (brushite grains) close to the percolation threshold p_c as we speculated in Sec. IV. Then the effective static conductivity is determined by the lowest contact conductivity $\sigma_c \cong \sigma_0 \exp(-\lambda)$. At finite frequency ω, the intergranular capacitances shunt the contact conductivities. The dispersion of the effective conductivity begins when the lowest conductivities are shunted by the capacitance, which occurs for frequencies $\omega > \sigma_c$. Considering the percolating system at $p = p_c$ we have shown [see discussion at Eq. (21)] that the imaginary part of the complex resistivity is maximum for the frequency ω_0
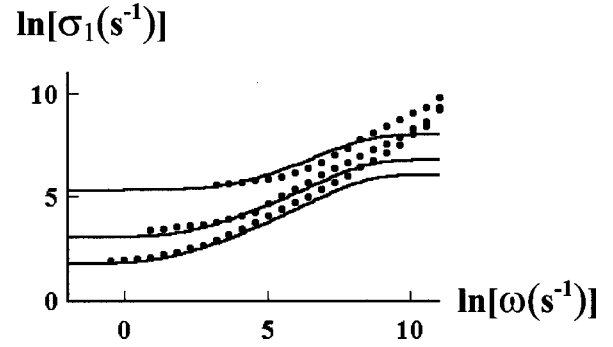
$\cong 2\sigma_c \propto \sigma_0 \exp(-\lambda)$. Therefore, the relaxation time τ_1 is proportional to $\tau_1 = 1/\omega_0 \propto \exp(\lambda)/\sigma_0$. When concentration p increases above the percolation threshold, we have a larger choice of conducting elements in the system to build up the conducting channels. Still, the contacts between the grains which are essential for the effective conductivity, can be considered as connected in series but the lowest contact conductivity increases. The lowest contact conductivity (critical conductivity), which is important for the effective conductivity can be written as $\sigma_c = 1/\rho_c(\omega \to 0) \cong \sigma_0 \exp[-\lambda(p_c/p)]$ [see Eq. (15)]. Correspondingly, the relaxation time $\tau_1 \propto 1/\sigma_c \propto \exp[\lambda(p_c/p)]/\sigma_0$ decreases exponentially when the concentration p of the brushite grains increases. When the concentration p increases further, the lowest static conductivities in the system may be shunted not only by their own capacitances but by the intergranular capacitances between other brushite grains. These contact conductivities do not participate in dc conductivity but they become important for frequencies larger than the critical conductivity $\omega > \sigma_c$. Then the relaxation time τ saturates somewhat for $p > 0.6$.

In Fig. 16 we show the frequency dependence of the real part σ_1 of the complex effective conductivity σ_e for the concentrations $p = 0.4$, 0.3, and 0.27. The high frequency part of the measurements corresponding to the condition $\omega > 1/\tau_1$ is more reliable for these lowest concentrations. We observe from Fig. 16 that the beginning of the dispersion of $\sigma_1(\omega)$ shifts to larger frequencies when increasing the concentration p and that the exponent α, defined by $\alpha = \max\{\partial \ln[\sigma_1(\omega)]/\partial \ln(\omega)\}_\omega$, is different for different concentrations. We compare the experimental data with results given by Eq. (30), obtained in Sec. IV in dimensionless form. For the real composites, this equation takes the following form:

$$\sigma_e(p,\omega) = \sigma_0 \sigma_e^*(p, \omega/\omega^*), \qquad (31)$$

where the dimensionless conductivity $\sigma_e^*(p, \omega/\omega^*)$ is given by Eq. (30), conductivity $\sigma_0 = 4.0 \times 10^5$ sec^{-1} was determined above from the behavior of static conductivity $\sigma_e(p,0)$, and parameter ω^* is a characteristic frequency. The parameters $p_c = 0.23$, $A = 0.035$, $B = 2.1$, and $\lambda = 10.1$ in Eq. (31) are the ones used to reproduce the static conductivity $\sigma_e(p,0)$ (see Fig. 13). Therefore, we have only one fitting
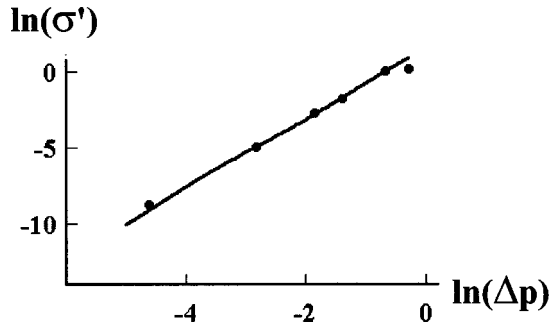
FIG. 17. Effective static conductivity of the percolating system with exponentially distributed local conductivity. ●: wet brushite composites, line is given by Eq. (29) for $\lambda = 7.9$, $\omega = 0$, $A = 0.035$, $B = 2.1$.

FIG. 18. Nyquist plot of the reduced resistivity ρ' for the wet brushite composites at two different concentrations. ●: $p = 0.25$ and ◆: $p = 0.76$. The curves are obtained from Eq. (29) taking into account the conductivity of the brushite grain itself given by Eq. (32).

parameter ω^* which we find equals $\omega^* = 6.6 \times 10^3$ sec^{-1}. Thus the obtained effective conductivity $\sigma_e(p, \omega)$ is in agreement with the experimental data for the low frequency region in Fig. 16, but it saturates at higher frequencies while the measured conductivity grows monotonically. This discrepancy may be due to the conductivity of the brushite grains themselves which we have not taken into account. To be more precise, we do not take into account the conductivity of the absorbed water layer around a brushite grain assuming that its impedance is much smaller than the contact impedance. For the frequencies $\omega > 1/\tau_1$ the ratio of imaginary to real parts of the effective conductivity, inverse loss tangent, becomes larger than 1 and the current in the contact flows mainly through the intergranular capacitance. Then the grain conductances which are in series with the contacts can lead to an increase of the real part of the effective conductivity.

B. Wet brushite composites

To verify the above suggestion we have prepared another series of wet brushite composites in the manner described above. The static conductivity of wet samples is about two orders of magnitude larger than that of dry samples. The reduced static conductivity of the wet composites is again in good agreement with scaling equation (29), as shown in Fig. 17, where percolation threshold $p_c = 0.24$ and parameter λ is now equal to $\lambda = 8.1$. The static conductivity σ_e at the concentration $p = 0.8$, which has been taken as a reference, is $\sigma_e(p = 0.8) = 3.9 \times 10^5$ sec^{-1}. The decrease of the parameter λ in comparison with dry samples corresponds to the increase of the static conductivity: the better the contacts between the brushite grains the smaller their fluctuations.

The Nyquist plot of the complex impedance of wet samples plotted in Fig. 18 shows a well-developed kick in the high frequency part of the curve. We attribute this kick to the conductivity of the brushite grains and include this conductivity in series with the contact conductivity in Eq. (30). The usual procedure in the impedance spectroscopy for this situation is to fit the impedance of each element in the system by constant phase elements with the impedance given by Eq. (1). Instead, we take the conductivity of a brushite grain σ_g to be in the following form:
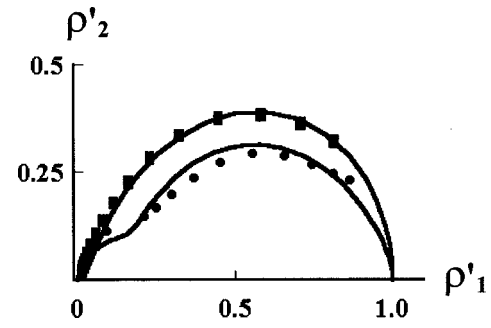
$$\sigma_g = \frac{i\sigma_g^* \lambda_g \omega}{\omega_g^* \ln\{[1 - i(\omega/\omega_g^*)\exp(\lambda_g)]/[1 - i(\omega/\omega_g^*)]\}},$$
$$(32)$$

where σ_g^*, ω_g^*, and λ_g are fitting parameters. This constant phase element (CPE) has the same number of parameters as the widely used CPE given by Eq. (1). In contrast to the old one, the suggested CPE has proper asymptotic behavior $\sigma \propto \omega^\alpha$ for the frequencies $\omega_g < \omega < \omega_g \exp(\lambda_g)$ with exponent α connected to the damping parameter β by Eqs. (20) and (22). We suppose that parameters σ_g^*, ω_g, and λ_g are the same for all brushite grains and connect the CPE's given by Eq. (32) in series with each contact conductivity. The Nyquist plot of such a system depends on the ratio of the parameters σ_g^*, ω_g^* to that for a contact between grains. A good fit gives the values $\lambda_g = 6.0$, $\sigma^*/\sigma_g^* = 0.14$, and $\omega^*/\omega_g^* = 1.5 \times 10^2$. Thus, we obtain reasonable agreement with the experimental data in Fig. 18. However, due to our hypotheses, the conductivity of one brushite grain cannot be found unambiguously from our experimental data. The purpose of the theoretical curve in Fig. 18 is to demonstrate that the behavior of the effective impedance can be rather complicated, even if each component of the system has conductivity that obeys the universal behavior. That is, each component of our system has a Nyquist plot in the form of the depressed semicircle with damping parameter $\beta \cong 0.4$ while the resulting plot is rather sophisticated.

VI. DISCUSSION: APPLICATION OF THE THEORY TO OTHER INHOMOGENEOUS SYSTEMS

Our theory reproduces the main features of the impedance spectroscopy of the brushite composites, at least qualitatively. The theoretical approach developed in this work can be applied to other inhomogeneous ionic conductors. Brushite composites are somewhat artificial systems since we introduce a well-defined parameter, namely, the concentration of an insulating component—polymer grains. This has been done in order to verify the theory.

One of the inhomogeneous systems with ionic conductivity to which our theory can be applied is porous sedimentary rocks whose pores are filled with water (see Refs. 15 and 36, and references therein). The conductivity behavior of the rocks implies that the pore space is infinitely connected

down to zero porosity. Sen *et al.* suggested that pores form fractal or self-similar structures. The bulk conductivity of the porous rocks can be attributed to the interlayer between the rock itself and the water-filled pore. In this interlayer, the water can easily dissociate in the manner discussed in Sec. II making proton conductivity along the interlayer possible. Since the pores have a variety of sizes and shapes, the local conductivity might be suggested to fluctuate in exponentially large range. If we adopted the suggestion that pores, i.e., conducting channels, form some fractal or self-similar structure the result of the developed theory can be taken into account for the complex impedance behavior of brine saturated rocks. Thus the strongly increasing behavior of the real dielectric constant at low frequencies, seen in many of these porous rocks, resembles that of the brushite composites shown in Fig. 5. Certainly, the structures of the pores do not necessarily match the structures of the percolation clusters, a fact which should be considered carefully for a quantitative analysis of the impedance behavior.

We have shown that it is very instructive to compare the results given by the Nyquist plot and the behavior of the effective conductivity σ_e (or resistivity) at sufficient high frequencies $\omega \gg 1/\tau_1$, where τ_1 is the effective relaxation time. We propose that as soon as the Nyquist plot is a well-defined depressed semicircle, the high frequency conductivity behaves as a power law $\sigma_e \propto \omega^\alpha$ and vice versa [see Eqs. (19) and (21) to compare the corresponding time and frequency scales]. A change in the relaxation time τ_1 will lead to a corresponding variation of the exponent α according to Eq. (25). When the relaxation time increases, the exponent α should also increase, approaching its ''universal'' value $\alpha = 1$. Note that the damping parameter β should reach its universal value $\beta = \ln(5)/4$ much earlier. In such a way, the effective parameter λ_e and, therefore, the distribution of the local conductivities, can be determined.

This approach can be generalized to inhomogeneous systems with *electronic* conductivity, e.g., metal-dielectric percolating systems in the vicinity of (or below) the percolation threshold. The exact nature of the contact conductivities is not important: it may be quantum tunneling (direct or hopping) or just bad contacts. As soon as the static conductivity is smaller (by several orders of magnitude) than the conductivity of the metal component, the frequency behavior should be as shown on Figs. 4 and 5. Then exponent α changes with the relaxation time according to Eq. (25). Indeed, in a very recent experiment,[36] authors report that the behaviors of the real parts of the effective conductivity and effective dielectric constant are very similar to those in Figs. 4 and 5. The parameter λ may be very large for processes involving quantum tunneling. Thus, substituting the experimental value of exponent $\alpha = 0.95$ given in Ref. 37 for some samples in Eq. (20), we obtain the effective parameter $\lambda_e \sim 80$. Moreover, one can observe the variation of the exponent α with relaxation time τ. As in brushite composites, the relaxation time in these systems depends on the concentration p of the conducting components.

The application of the concept of local conductivity to amorphous and heavily doped semiconductors is somewhat controversial since these systems have an essentially microscopic disorder. Therefore, our theoretical results may not be directly applied to these systems. Still we believe that corre-

lation has to be made between numerous $\sigma(\omega)$ data for these systems and their rearrangement in form the Nyquist plot. It would be very interesting to see if Eqs. (20) and (22) provide a qualitative description of the impedance spectroscopy data for amorphous and heavily doped semiconductors.

VII. CONCLUSIONS

We have performed a comprehensive theoretical and experimental study of brushite percolating composites which have ionic conductivity. The investigation of the percolating systems allows us to introduce a well controlled parameter, namely, the concentration of the conducting component, and to study the dispersive behavior of the complex impedance as a function of this well controlled parameter. The Nyquist plot of the complex impedance is a depressed semicircle whose points, for all concentrations of the conducting component, are on a single curve. Along with this, the relaxation time increases exponentially when the concentration of the brushite grains decreases towards the percolation threshold. The static conductivity dependence shows the power-law behavior typical for percolating systems but, in contrast to usual conductor-dielectric composites, the power-law behavior holds for the entire concentration range. At finite frequency, the conductivity has a dispersion behavior that can also be fitted by some power law with an exponent which depends, in general, on the concentration of brushite.

We introduced a microscopical model for brushite composites with local complex conductivities, the real part being distributed in an exponentially wide range. A computer simulation of the system has been performed. We use a very efficient algorithm to tackle the problem of a composite with exponentially distributed local conductivities. In addition to the calculation of the effective properties, our algorithm shows that a percolating system is self-similar at the percolation threshold. The computer simulations reproduce the main features of the experimentally observed complex impedance behavior in brushite composites.

Starting from our computer results, we developed a scaling theory for the effective complex conductivity (impedance). The most important feature of our system is that the scale of the spatial inhomogeneity of the local fields and currents remains large for any concentration of the conducting component. This allowed us to suggest a scaling equation for the effective conductivity. This equation exactly reproduces the unusual behaviors of the static conductivity observed either experimentally or numerically. This equation gives the frequency behavior of the complex impedance in the entire concentration range. The developed theory links the impedance spectroscopy data to the internal structure of the system. Thus, it predicts that observed exponents for the dispersion behavior of the complex impedance are connected and dependent, in a rather simple way, on the distribution of the local parameters. The theoretical results obtained in this work can be used to describe the effective properties of any system with an exponentially distributed local conductivity, i.e., most of the inhomogeneous ionic conductors and some disordered electronic conductors as well.

ACKNOWLEDGMENT

[1] A. K. Jonscher, *Dielectric Relaxation of Solids* (Chelsea Dielectric Press, London, 1983); R. Coelho and B. Aladenize, *Les Diélectriques* (Hermes, Paris, 1993).

[2] A. L. de Olivera, O. de O. Damasceno, and J. de Olivera, Mater. Res. Bull. **21**, 877 (1986).

[3] U. Lauter and J. Maier, Ber. Bunsenges. Phys. Chem. **96**, 111 (1992).

[4] A. Zaban, E. Zinigrad, and D. Aurbach, J. Chem. Phys. **100**, 3089 (1996); R. P. Buck and C. Mundt, J. Chem. Soc., Faraday Trans. **92**, 3947 (1996); **100**, 3089 (1996).

[5] A. Le Mehaute and G. Crepy, Solid State Ionics **9&10**, 17 (1983); A. Le Mehaute, J. Stat. Phys. **36**, 665 (1984); A. Le Mehaute, L. Picard, and L. Fruchter, Philos. Mag. B **52**, 1071 (1985); T. Hamaide, A. Cuyot, A. Le Mehaute, G. Crepy, and G. Marcellin, J. Electrochem. Soc. **136**, 3152 (1989); A. Le Mehaute, *Les Geometries Fractales* (Hermes, Paris, 1990).

[6] J. Ross Macdonald, *Impedance Spectroscopy* (Wiley, New York, 1987).

[7] A. Beevers, Acta Crystallogr. **11**, 273 (1958); D. W. Jones and J. A. S. Smith, J. Chem. Soc. **58**, 1414 (1962); L. C. Herring, J. Urol. (Baltimore) **88**, 545 (1962); B. Dickens, *Symposium on Structural Properties of Hidroxyapaite and Related Compounds*, edited by W. E. Brown (Gordon, New York, 1971); N. A. Curry and D. W. Jones, J. Chem. Soc., **67**, 3725 (1971).

[8] L. Tortet, J. R. Gavarri, and G. Nihoul, Solid State Ionics **89**, 99 (1996).

[9] L. Tortet, J. R. Gavarri, G. Nihoul, J. M. Falcons, and F. Rouquerol, Eur. J. Solid State Inorg. Chem. **33**, 1199 (1996).

[10] L. Tortet, J. R. Gavarri, G. Nihoul, and A. J. Dianoux, J. Solid State Chem. (to be published).

[11] J. C. Wang and J. B. Bates, in *Solid State Ionics*, edited by G. Nazri, R. A. Huggins, and D. F. Shriver, MRS Symposia Proceedings No. 135 (Materials Research Society, Pittsburgh, 1989).

[12] J. C. Wang and J. B. Bates, Solid State Ionics **50**, 75 (1992).

[13] J. B. Bates and J. C. Wang, Solid State Ionics **28-30**, 115 (1988).

[14] E. H. Stanley, *Introduction to Phase Transitions and Critical Phenomena* (Oxford University Press, Oxford, 1971); S. Ma, *Modern Theory of Critical Phenomena* (Benjamin, London, 1976); P. M. Chaikin and T. C. Lubensky, *Principles of Condensed Matter Physics* (Cambridge University Press, Cambridge, 1995).

[15] J. P. Clerc, G. Giraud, and J. M. Luck, Adv. Phys. **39**, 191 (1990); D. Stauffer and A. Aharony, *Introduction to Percolation Theory*, 2nd ed. (Taylor and Francis, Philadelphia, 1991); D. J. Bergman and D. Stroud, Solid State Phys. **46**, 147 (1992).

[16] A. K. Sarychev and F. Brouers, Phys. Rev. Lett. **73**, 2895 (1994).

[17] J. Jacquelin, Rev. Gen. Electr. **47**, N1 (1987).

[18] S. R. Elliot, Adv. Phys. **36**, 135 (1987).

[19] G. A. Niklasson, J. Appl. Phys. **62**, R1 (1987).

[20] J. P. Clerc, A. N. Lagarkov, A. P. Pluhin, and A. K. Sarychev (unpublished).

[21] R. A. Robinson and R. H. Stokes, *Electrolyte Solutions* (Butterworths, London, 1970).

[22] A. M. Dykhne (private communication).

[23] F. Uchikawa and K. Shimamoto, Solid State Ionics **21**, 1 (1986).

[24] E. Gileady, *Electrode Kinetics for Chemists, Chemical Engineers and Material Scientists* (VSH, Oxford, 1989); G. Milazzo, *Electrochimie* (Dunod, Paris, 1969), Chap. IV.

[25] D. J. Frank and C. J. Lobb, Phys. Rev. B **37**, 302 (1988).

[26] A. P. Vinogradov and A. K. Sarychev, Zh. Eksp. Teor. Fiz. **85**, 1144 (1983) [Sov. Phys. JETP **58**, 665 (1983)].

[27] A. K. Sarychev, D. J. Bergman, and Y. M. Strelniker, Phys. Rev. B **48**, 3145 (1993).

[28] R. Boite and J. Neirynck, *Théorie des Réseaux de Kirchhoff* (Dunod, Paris, 1983).

[29] A. K. Sarychev and A. P. Vinogradov, J. Phys. C **14**, L487 (1981); Y. Gefen, A. Aharony, B. B. Mandelbrot, and S. Kirkpatrick, Phys. Rev. Lett. **47**, 1771 (1981); B. B. Mandelbrot and J. Given, *ibid.* **52**, 1853 (1984); L. de Arcangelis, S. Redner, and A. Coniglio, Phys. Rev. B **31**, 4725 (1985).

[30] B. B. Mandelbrot, *The Fractal Geometry of Nature* (Freeman, San Francisco, 1982).

[31] A. Coniglio, Phys. Rev. Lett. **46**, 250 (1981).

[32] A. B. Pike and H. E. Stanley, J. Phys. A **13**, 457 (1980).

[33] V. Ambegaokar, B. I. Halperin, and J. S. Langer, Phys. Rev. B **4**, 2612 (1971); B. I. Shklovskii and A. L. Efros, *Electronic Properties of Doped Semiconductors* (Springer-Verlag, Berlin, 1984); P. Le Doussal, Phys. Rev. B **39**, 881 (1989).

[34] I. Webman, J. Jortner, and M. H. Cohen, Phys. Rev. B **11**, 2885 (1975); G. G. Bartrouni and A. Hansen, J. Stat. Phys. **11**, 2885 (1988).

[35] L. D. Landau and I. M. Lifshitz, *Electrodynamics of Continuous Media*, 2nd ed. (Pergamon, Oxford, 1984), Chap. 2, Sec. 9.

[36] P. N. Sen, W. C. Chew, and D. Wilkinson, in *The Physics and Chemistry of Porous Media*, AIP Conf. Proc. No. 107, edited by D. L. Johnson and P. N. Sen (AIP, New York, 1983), p. 52.

[37] J. Wu and D. S. McLachlan, Phys. Rev. B **56**, 1236 (1997).